PHOTONIC SENSORS / Vol. 16, No. 2, 2026: 9560015

Advances in InX (X: As, Sb) Quantum Dots Infrared Photodetectors

Huiling TAI*, Wenxin ZENG, Zaihua DUAN, and Yadong JIANG

State Key Laboratory of Electronic Thin Films and Integrated Devices, University of Electronic Science and Technology of China, Chengdu 611731, China

*Corresponding author: Huiling TAI E-mail: taitai1980@uestc.edu.cn

Abstract: Infrared photodetectors exhibit significant applications in the fields, such as the defense military, industry, and consumer electronics. Leveraging the advantages, like adjustable bandgap, high carrier mobility, solution processing ability, and low cost, the InX (X: As, Sb) quantum dots (QDs) emerge as the promising candidate "green" materials for next-generation infrared photodetectors, compared to Hg- and Pb-based infrared QDs. However, the controllable synthesis and improved photoelectric properties of InX QDs are limited by the strong covalent bonding between indium and heavy pnictogens and the high-density surface defects, resulting in device metrics that are yet to match those of their toxic counterparts. In recent years, the synergistic innovations in the synthesis technique, ligand engineering, and device structure design have led to significant improvements in the performance of InX QDs infrared photodetectors. This review focuses on the advances of InX QDs-based infrared photodetectors. Firstly, various synthetic methods of InX QDs are reviewed. Secondly, the performance optimization strategies (synthesis process optimization, surface passivation, and device structure design) of InX QDs infrared photodetectors are discussed in detail. Finally, the challenges and prospects for future research in InX QDs infrared photodetectors are proposed. Through a comparative analysis of the InAs and InSb QDs systems, this review establishes a clear "material-to-device" optimization path to unlock the full potential of InX QDs photodetectors and accelerate the development of stable, efficient, and eco-friendly infrared devices.

Keywords: Quantum dots; InAs; InSb; infrared photodetector

Citation: Huiling TAI, Wenxin ZENG, Zaihua DUAN, and Yadong JIANG, "Advances in InX (X: As, Sb) Quantum Dots Infrared Photodetectors," *Photonic Sensors*, 2026, 16(2): 9560015.

1. Introduction

As core components to realize the conversion from light into electrical signals, the photodetectors play a crucial role in numerous applications, such as optical communication, imaging, and industrial detection [1–3]. The increasing complexity of detecting environments and target objects places higher demands on photodetectors, especially infrared photodetectors with the detection capability across the near infrared (NIR, 0.75 μm–1.4 μm) to short wave infrared (SWIR, 1.4 μm–3 μm) regions [1]. Infrared photodetectors can perform clear target recognition in low light/nighttime environments,

Received: 28 August 2025 / Revised: 13 November 2025
©The author(s) 2026. Published by Tsinghua University Press. This is an open access article under the Creative Commons Attribution 4.0 International License (http://creativecommons.org/licenses/by/4.0/)
DOI: 10.26599/PhoS.2026.9560015
Article type: Review

endowing them with irreplaceable applications in defense military, industry, and consumer electronics [4]. At present, the commercial infrared photodetectors mainly rely on bulk semiconductor materials with a narrow bandgap, including Ge, InGaAs, and HgCdTe [5, 6]. Nevertheless, their large-area fabrication and array integration are limited by a complex fabrication process and high cost [7–11]. Quantum dots (QDs) have garnered intensive attention in the field of infrared photodetectors owing to their size-tunable bandgap, high absorption coefficient, solution processability, and low synthesis cost. To date, the most extensively studied QDs are lead and mercury chalcogenide QDs (such as PbS, PbSe, HgSe, and HgTe) [12]. Remarkably, recent advancement in PbS QDs-based photodetectors has reached a record-breaking specific detectivity (D^*) surpassing 10^{14} Jones [13]. However, their further commercial applications and transformation may be hindered by toxic elements Pb and Hg, which belong to the category of highly toxic heavy metals specified by the European Union Restriction of Hazardous Substances (RoHS) Directive [14]. Therefore, it is significant to develop eco-friendly QDs alternatives.

III-V semiconductor InX (X: As, Sb) QDs serve as the "green" substitute without extremely hazardous heavy metal elements (Pb and Hg) that are harmful to the ecological environment, and exhibit the same zinc blende crystal structure and similar optoelectronic properties [15]. InAs has a direct bandgap of 0.354 eV, low permittivity, small effective carrier mass, small exciton binding energy, and high photoactivity [16]. Although much progress has been made in InAs QDs-based infrared photodetectors, due to the instability of large-size InAs QDs, the photoresponse range is hard to exceed 1 500 nm. Compared to InAs, the InSb possesses a narrower direct bandgap of 0.17 eV, a larger exciton Bohr radius (60 nm), and a higher carrier mobility of 7.7×10^4 $cm^2\cdot V^{-1}\cdot s^{-1}$, which are more promising in SWIR photodetection [17]. The strong covalent bonding between the III-V group atoms makes InX QDs more chemically stable compared to the ionic compound semiconductor QDs, but it also brings difficulties to the controllable synthesis of InX QDs and the performance improvement of InX QDs-based infrared photodetectors. For instance, the selection of precursors for synthesis is limited. A few available precursors, like tris-trimethylsilyl arsine ($(TMS)_3As$ or $(TMSi)_3As$), show strong reactivity, which poses significant challenges in controlling the size monodispersity of InX QDs [18–22]. Some stibium precursors are unstable and require independent synthesis and long-term purification before use. The disparate reduction kinetics between groups III and V elements, coupled with mismatched reaction temperatures and reducing agents, often leads to the formation of synthetic byproducts, such as indium nanocrystals (NCs) [23]. In addition, numerous dangling bonds on the surface of InX QDs are prone to oxidation. It is easy to introduce deeper trap states within the bandgap, finally generating severe carrier recombination.

In recent years, fruitful progress has been made in addressing these challenges of InX QDs through the collaborative development of the synthesis process, surface passivation, and device structure engineering (Fig. 1). Skorotetcky *et al.* [24] introduced 1,1,3,3,5,5-hexamethyltrisiloxane (HMTS) as a novel stable and non-toxic hydrosilane reducing agent in the synthesis of InAs QDs. This study achieved the shape control of the tetrahedral shape and tunable absorption of the excitonic peak up to 1 550 nm of InAs QDs. Wang *et al*. [25] proposed another stepwise crystallization synthetic strategy for InSb QDs with the unprecedented absorption spectrum extending 3 000 nm and a remarkably low size distribution deviation of 5.8% without size-selective precipitation. The performance of the InX QDs-based infrared photodetectors also achieved a breakthrough. Xia *et al*. [26] developed a mixed-halide passivation strategy for large InAs

QDs with chloride and bromide. The peak external quantum efficiency (EQE) of the InAs QDs-based photodetector was increased to 75% at 1 140 nm under the 0.5 V bias voltage, while improving the stability of the photodetector operation. Current reviews about InAs and InSb QDs-based infrared photodetectors largely analyze these materials in isolation, while neglecting systematic discussions on their similarities and differences [27–31]. In the review papers covering multiple different QDs photodetectors, there is also a lack of separate discussions on optimization strategies and performance parameters for InX quantum dot infrared photodetectors. As shown in Fig. 2, this review focuses on the InAs and InSb QDs and their infrared photodetectors. Firstly, the basic synthesis methods are introduced, and then the recent progress of performance optimization strategies for InAs and InSb QDs-based infrared photodetectors is discussed in detail, including the synthesis process optimization, surface passivation, and device structure design. Finally, the challenges and

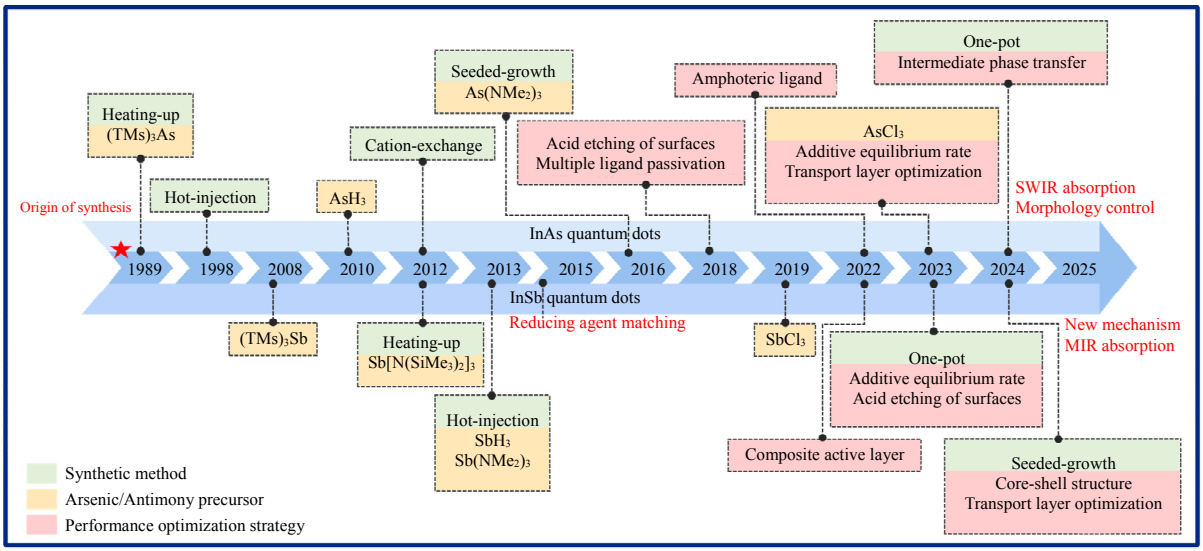


Fig. 1 Roadmap for the development of InX QDs.

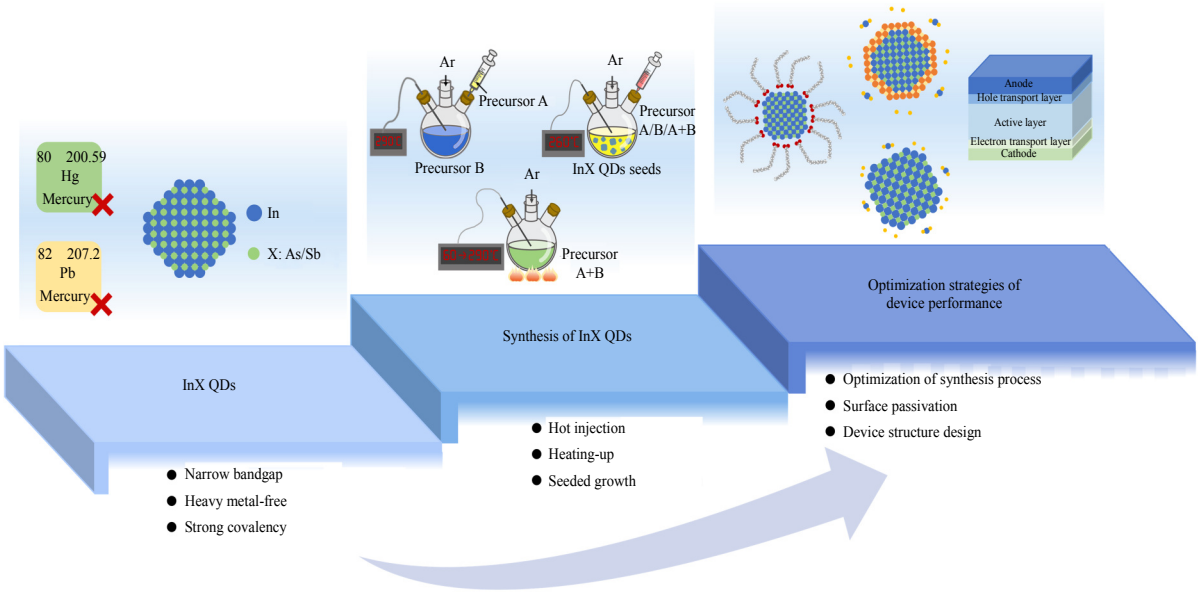


Fig. 2 Overview diagram of synthesis methods of InX QDs and performance optimization strategies of InX QDs infrared photodetectors.

prospects of InAs and InSb QDs infrared photodetectors are summarized and discussed. This review is essential for advancing the practical implementation of InX QDs infrared photodetectors.

2. Synthesis of the InX QDs

To overcome the synthetic challenges of InX QDs constrained by high covalency, a synergistic approach involving appropriate precursors, compatible reducing agents, and high synthesis temperatures is demanded to achieve controlled synthesis. With the development of the synthetic technology in the past few years, the in-depth understanding of the nucleation and growth mechanisms has further improved the size tunability, shape control, monodispersity, and stability of the InX QDs. Beyond the widely used hot-injection, other synthetic approaches, such as heating-up, seeded growth, and cation exchange, have been continuously emerging.

2.1 Hot-injection

The most classic hot-injection method involves rapidly injecting one precursor into another vigorously stirred hot precursor [32]. This transient process generates an immediate supersaturation of monomers, inducing a burst of nucleation, followed by a rapid decrease in the monomer concentration to suppress further nucleation while promoting QDs growth. Such an approach effectively decouples the nucleation and growth stages, enabling precise control over the QDs size distribution [33]. With advancing insights into the reaction kinetics of the QDs nucleation and growth, this method has evolved from the conventional single-source rapid injection to more sophisticated approaches, including single-source continuous injection and dual-source hot-injection strategies.

Inspired by the dehalosilylation reaction in GaAs synthesis, $(TMS)_3As$ and its analogs (e.g., tris(trimethylgermyl)arsine [$(TMGe)_3As$], tris(triethylgermyl)arsine [$(TEGe)_3As$] were introduced into the early synthesis of the InAs QDs [34]. For single source hot-injection, these As precursors often react quickly with indium sources due to high reactivity. The rapid depletion of monomers limits the quality of the QDs. Franke *et al*. [35] achieved the precise control over reaction kinetics through the continuous single-source injection of $(TMGe)_3As$ precursor, obtaining larger InAs QDs with excitonic absorption peaks in the NIR region [Fig. 3(a)]. However, the high reactivity, flammability, toxicity, and high cost of $(TMS)_3As$ and its analogs impede the synthesis and subsequent processing of InAs QDs. It is necessary to develop a safer and more reliable arsenic precursor.

AsH_3 has been explored as a gaseous precursor in some studies. For instance, Zhang *et al*. [36] synthesized high-quality InAs NCs with a shift in the first exciton peak from 650 nm to 800 nm by using AsH_3 generated via Zn_3As_2 [Fig. 3(b)]. However, the instability of the monomer formed from AsH_3 led to the dissolution of the synthesized products upon prolonged growth time. Additionally, the toxicity and instability of AsH_3 made it an unsuitable replacement for $(TMS)_3As$.

The use of aminophosphines as alternatives to tris(trimethylsilyl)phosphine in the synthesis of InP QDs has sparked interest in exploring aminarsines tris(dimethylamino)arsine [$As(NMe_2)_3$] as reliable substitutes for $(TMS)_3As$ [37]. As a commercially available, low-cost, and safely handled arsenic precursor, $As(NMe_2)_3$ does not react directly with conventional indium sources [e.g., $InCl_3$ or $In(OAc)_3$], necessitating additional reducing agents to regulate the release of As^{3-}. As shown in Fig. 3(c), Srivastava *et al*. [38] compared the effect of four reducing agents [$P(NEt_2)_3$, DIBAL-H, DMEA-AlH_3, and $LiEt_3BH$] on the precursor conversion kinetics and the final size distribution of InAs QDs. They found that selecting the appropriately active DMEA-AlH_3 as a reducing agent could yield highly monodisperse InAs QDs comparable in quality to those prepared with $(TMS)_3As$. In 2024, a new

hydrosilane reducing agent, HMTS, was introduced [24]. With the assistance of In and Zn halogenides as the Lewis acid catalysts, it overcame the slow precursor conversion caused by the weak reducing agents, enabling high-quality large-sized InAs QDs with absorption peaks tunable up to 920 nm. Future research on hydrosilanes with varying structures, numbers of reactive sites, and polar-nonpolar functionalities will further advance the synthesis of InAs QDs.

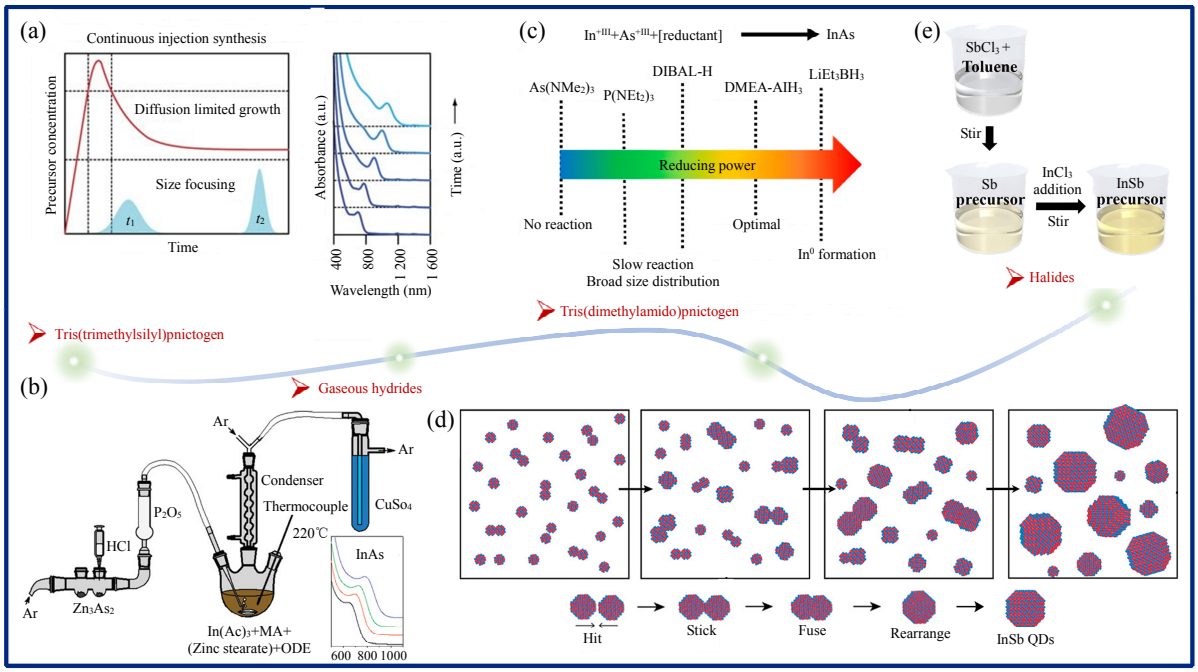


Fig. 3 Evolution of precursor types and injection strategies in the conventional hot injection approach of InX QDs: (a) the schematic diagram of the temporal evolution of precursor concentration and the absorption spectrum of the obtained InAs QDs during a continuous injection [35], (b) experimental setup diagram for the synthesis of InAs QDs using the gaseous precursor AsH_3 [36], (c) schematic representation of the influence of the reducing ability of different reducing agents on the synthesis of InAs QDs [38], (d) schematic illustration of the innovative aggregative growth mechanism for the synthesis of InSb QDs [43], and (e) the preparation process of the "dual-source" precursor through commercially available halides ($InCl_3$ and $SbCl_3$) [46].

As a member of III-V QDs, the development of precursors for InSb QDs follows a similar trajectory to that of InAs QDs, starting with the desilylation reaction of tris(trimethylsilyl)antimony [$(TMS)_3Sb$]. In 2008, Evans *et al*. [39] developed a synthetic route for $(TMS)_3Sb$ and used it as a precursor to synthesize InSb QDs via a colloidal approach. Subsequently, the gaseous precursor SbH_3 was also considered. Maurice *et al*. [40] employed potassium antimonyl tartrate reduced in an acidic medium to generate SbH_3 as a precursor, obtaining 8.8 nm InSb NCs without reducing agents. However, the InSb QDs synthesized using these two precursors did not exhibit clear excitonic absorption peaks. Moreover, $(TMS)_3Sb$ is far less stable than phosphorus and arsenic analogs, and SbH_3 is highly toxic, making synthesis and post-treatment challenging.

In 2013, Yarema *et al*. [41] proposed a new synthetic route combining commercially available tris(dimethylamido)antimony [$Sb(NMe_2)_3$] and triindium(silylamide), achieving InSb QDs with shoulder peaks from 1 250 nm to 1 750 nm and a size distribution of 10%–15% without size selection. By adjusting the In-to-Sb precursor ratio, they also achieved polymorphic and polytypic control over InSb QDs. However, due to the air and moisture sensitivity of the metal silylamides, it required self-synthesis and lengthy purification, and this approach was not suitable for the widespread use. Tamang *et al*. [42] proposed a simple hot-injection

method using only commercially available $InCl_3$ and $Sb(NMe_2)_3$, with reducing agents, such as $Li[N(SiMe_3)_2]$, nBuLi, and $LiBHEt_3$. However, this method only yielded polydisperse InSb QDs with diameters of 3 nm–6 nm, displaying featureless absorption spectra. The outcome was attributed to the imbalanced reduction kinetics of the two elements, leading to the precipitation of Sb NCs and In-rich InSb QDs. To address this issue, Busatto *et al*. [43] innovatively utilized the Lewis acid-base properties of $Sb(NMe_2)_3$ and $InCl_3$ to prepare a "dual-source" precursor containing In-Sb bonds for hot injection, which facilitated the formation of InSb QDs. Additionally, their study revealed a non-classical nucleation and growth pathway involving QDs aggregation, as shown in Fig. 3(d). Unlike the classical nucleation theory, in this non-classical pathway, precursors were completely converted into monomers via rapid co-reduction, depleting the precursor reservoir entirely. The InSb precursor complex was directly transformed into small $[InSb]_n$ molecular clusters. Due to their high mobility and adjacent NCs collide and aggregate, the InSb QDs were formed through structural remodeling. Building on this, Peng *et al*. [44] employed dual-source continuous injection and size selection to eliminate fused particles formed during synthesis, which contributed to trap-state tailing. This approach yielded high-quality InSb QDs with a sharp first excitonic absorption peak at 1 160 nm and a peak-to-valley ratio of 1.65. Kwon *et al*. [45] reported a hot-injection synthesis of InSb QDs using In(I)X (X=Cl, Br, and I) and $Sb(NMe_2)_3$ as precursors, where In(I)X served a dual role as both an indium source and a mild reducing agent, eliminating the need for strong reducing agents. The excitonic absorption peaks of these QDs could be tuned across a broad range of 630 nm–1 890 nm.

Furthermore, as depicted in Fig. 3(e), He *et al*. [46] employed more accessible $InCl_3$ and $SbCl_3$ commercial materials as the "dual-source" precursors and synthesized InSb QDs with an excitonic absorption peak at 1 700 nm via hot injection. The simplicity of operation and good controllability of the product have led to this method being frequently employed to fabricate InSb QDs directly or with appropriate modifications.

2.2 Heating-up

For the hot-injection method, the quality of InX QDs is sensitive to the acceleration of solution mixing efficiency, precise temperature profiles, and injection rates. These factors become difficult to control during large-scale synthesis, finally compromising the controllable synthesis of QDs. In contrast, the heating-up method offers a simpler and reproducible alternative for industrial-scale QDs production, circumventing the limitations inherent to the hot-injection method [47–49]. In this scheme, all reactants are premixing at a low temperature, followed by gradual heating to the reaction temperature to activate rapid precursor conversion, thereby promoting nucleation and growth. Despite its advantages, this method generally yields highly polydisperse QDs due to the overlap between nucleation and growth stages. To address these challenges, researchers have progressively refined the heating-up method to produce monodisperse InX QDs. The key strategies include the careful selection of precursors and additives, as well as controlled heating rates, to decouple nucleation and growth stages.

For InAs QDs, in 1989, Wells *et al*. [50] first employed $InCl_3$ and $(TMS)_3As$ as precursors through the heating-up method to yield InAs NCs over several days. However, the prolonged reaction time and high reactivity of $(TMS)_3As$ led to unintended particle aggregation and by-products, which compromised the quantum confinement effect and optoelectronic performance of InAs QDs [51]. Das *et al*. [52] proposed an easily prepared and environmentally stable precursor $[(Me_3Si)_2N]_2AsCl$ to synthesize InAs QDs. With the improvement of the precursor stability, the introduction of reducing agents can effectively reduce the synthesis

temperature and reaction time of QDs. Unfortunately, the absorption spectrum still lacks features, indicating that the issue of monodispersity has not been addressed. Zhao *et al*. [53] reported the synthesis of III-V QDs, including InAs, InSb, and ternary $InAs_{1-x}Sb_x$ QDs, through a facile heating-up method, in which the mixtures were heated up by a heating mantle at 3 ℃/min to the reaction temperature [Fig. 4(a)]. Commercially available and chemically stable $InCl_3$ and $AsCl_3$ precursors were used to form InAs QDs with first excitonic absorption resonances tuned from 800 nm to 1 300 nm in the presence of the superhydride reducing agent. The above method required additional size-selective precipitation processes to obtain QDs with a relatively uniform size distribution. To further simplify the processing flow, Kim *et al.* [54] presented a synthetic strategy using zinc chloride-based reaction additives to alter the reaction path and improve the surface reaction rate. This modification led to distinct excitonic peaks with a peak-to-valley ratio of 0.78 in the NIR band, regardless of the follow-up process. Moreover, the zinc ion passivation of surface defects provided a promising solution for improving the optoelectronic properties of InX QDs. The heating-up method also made some achievements in the morphology control of InAs QDs. Sheikh *et al*. [55] utilized $InCl_3$ and AsI_3 halide precursors and $LiN(Si(CH_3)_3)_2$ reducing agent to achieve the synthesis of InAs colloidal nanorod QDs (CNQDs). At a higher temperature, the precursors first formed In nanoparticles, which acted as seeds to direct the growth in the [111] direction. By varying the amount of the reducing agent, the absorption peaks of these InAs CNQDs can be precisely tuned from 1 200 nm to 1 800 nm surpassing the practical barrier encountered by previous InAs QDs.

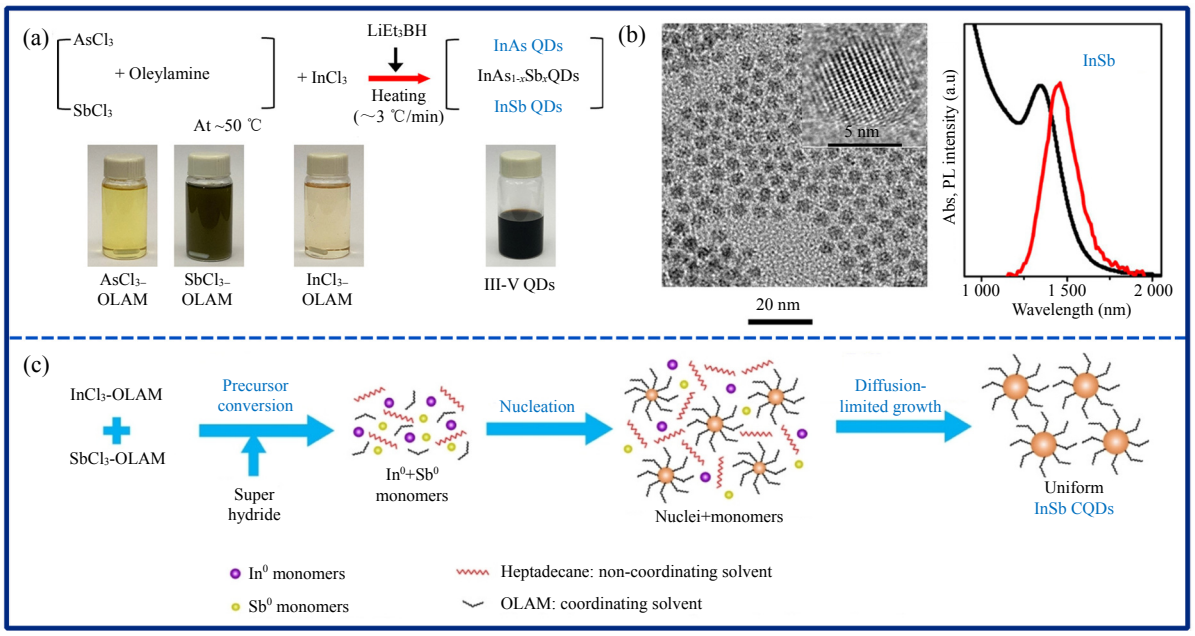


Fig. 4 Recent advances in the heating up synthetic method of InX QDs: (a) the reaction schematic and photographs of the precursors and product $InAs_{1-x}Sb_x$ QDs [53], (b) the TEM image and absorption (black) and photoluminescence (red) spectra of 3.8 nm InSb NCs synthesized by the heating-up method [56], and (c) the illustration of the InSb QD synthesis process including three stages of the precursor conversion, nucleation, and diffusion-limited growth [59].

In 2012, Liu *et al.* [56] reported the first colloidal synthesis of monodisperse and well crystallized InSb NCs. The mixture, including $InCl_3$, $Sb[N(SiMe_3)_2]_3$, and LiEt3BH, was heated to 260 ℃ at a rate of approximately 3 ℃/min and annealed for 20 minutes to obtain InSb NCs exhibiting well-resolved exciton absorption in the NIR spectrum range (1 200 nm–1 750 nm) [Fig. 4(b)].

Yarema *et al*. [41] synthesized InSb QDs using highly reactive element-nitrogen bonded precursors $In[N(SiMe_3)_2]_3$ and $Sb[NMe_2]_3$. These InSb QDs showed a size-tunable absorption in the NIR region of 1 500 nm–2 000 nm with a single peak/shoulder. Furthermore, they achieved zinc blende/wurzite polymorphism of InSb QDs controlled by the In/Sb molar ratio of precursors and first reported monodisperse InSb nanorods. But the InSb QDs obtained by this method had thick oxide layers, resulting in poor optical properties. Beyond precursors mentioned above, commercially available and chemically stable metal halide precursors, such as $InCl_3$ and $SbCl_3$, were also widely used [53, 57, 58]. Although various precursors and reducing agents had been tried, the obvious exciton absorption peak currently still depended on the size-selection process assistance. Controlling precursor reaction kinetics via additive incorporation (such as molecular [57] and metal halide additives [58]) was employed as an effective strategy to overcome this challenge. Zhang *et al*. [59] refined Zhao's heating-up method [53] to produce InSb QDs with narrow size distributions (<10%) and a sharp excitonic peak at 1 400 nm without size-selective post-treatment. Heptadecane, a non-functionalized high-boiling-point alkane incapable of InSb QDs surface binding, was introduced as an additional solvent into the reaction mixture. The non-coordinating solvent tuned the concentration of monomers to balance the nucleation and growth rates needed for obtaining large QDs. Moreover, with the steric hindrance, the heptadecane also facilitated a diffusion-limited growth regime by hindering the diffusion of monomers to the nuclei [Fig. 4(c)].

2.3 Seeded growth

The seeded growth is an improved method derived from the hot-injection technique, in which pre-synthesized nanocrystal seeds serve as templates for the precursor-mediated epitaxial growth. Compared to standard hot-injection and heating-up methods, it can effectively separate nucleation and growth stages. Although sacrificing the synthetic convenience, the seeded growth demonstrates remarkable advantages in the monodispersity improvement, size expansion, and morphology control of QDs [60]. Currently, the synthesis of InX QDs is commonly achieved by continuously injecting amorphous prenucleation clusters into the seed solution [61–63].

Jeong's group first synthesized InAs seeds and ultrasmall amorphous InAs nanoclusters through a hot-injection method using indium oleate and $(TMS)_3As$ [64]. As presented in Fig. 5(a), the InAs QDs exhibiting a pronounced exciton absorption peak across the ultraviolet-NIR spectrum were synthesized by injecting amorphous InAs nanocluster solutions into seeds at variable rates under the specific growth temperatures. Due to the inhibition of self-nucleation by seeds, smaller seeds grew faster than larger ones. And then the size distribution gradually narrowed, resulting in the final production of InAs QDs with good monodispersity [Fig. 5(b)]. Subsequently, this group further refined their prior methodology and successfully synthesized InAs QDs with a narrow size distribution (the standard deviation less than 3.7%) utilizing dioctylamine co-surfactant [65]. Furthermore, a molecular diffusion-based growth model for the continuous synthesis of InAs QDs was proposed. Guided by this model, the InAs QDs with 1 600 nm peak absorption, which overcame the size limit of the QDs growth in solutions, were successfully synthesized by adjusting the reaction volume, precursor concentration, and injection rate [66]. Skorotetcky *et al*. [24] successfully synthesized the tetrahedral shape InAs QDs in the seeded growth approach using $InCl_3$, $As(NMe_2)_3$, and $ZnCl_2$, together with the HMTS, which achieved tunable absorption of the first excitonic peak up to 1 550 nm. It was also found that changing the temperature, injection rate, and the presence or absence of $ZnCl_2$ had little effect on the shape of the InAs QDs finally obtained, only resulting in

different arm widths and lengths.

The synthesis of InSb QDs follows the seeded growth approach for InAs QDs. Jee *et al*. [67] prepared In-oleate and Sb precursors using the oleic acid (OA), $InCl_3$, trioctylamine, and $(TMS)_3Sb$, and synthesized seeds, and cluster solutions. The cluster solutions at the room temperature were injected into a high-temperature seed solution at a constant injection rate [Fig. 5(c)]. With an increase in the cluster concentration, the average diameter of InSb QDs increased from 4.1 nm to 5.3 nm, and the exciton absorption peak reached 1 600 nm, which was more significant than the ones synthesized by the hot-injection method. By changing precursor composition during synthesis, the core-shell structured InX QDs, such as InAs/InZnP/GaP/ZnSe, InAs/CdSe/ZnSe, and InSb/InAs/ZnSe QDs, were readily prepared [35, 68, 69].

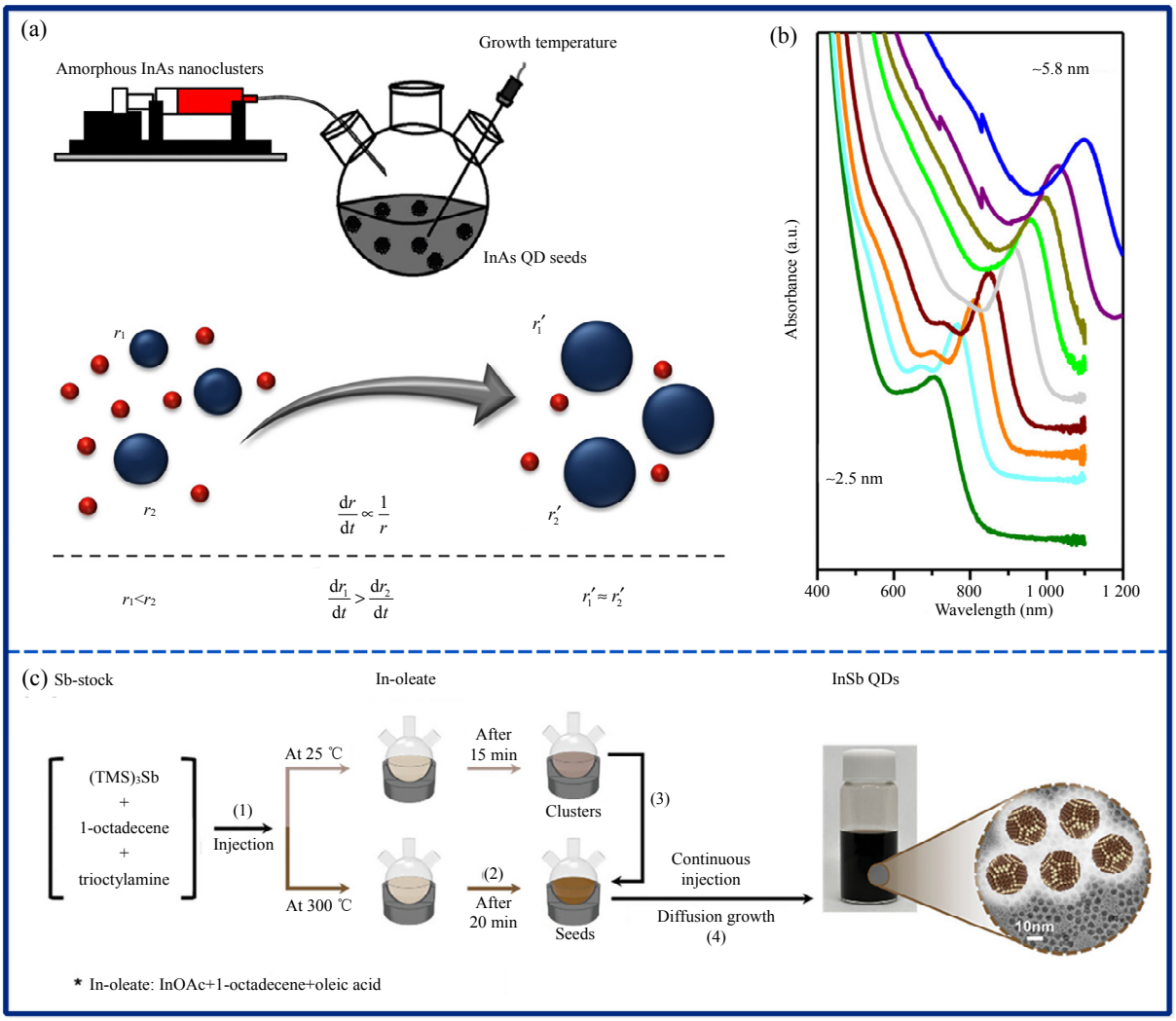


Fig. 5 Seeded growth synthesis of InX QDs: (a) the synthesis scheme of InAs QDs by the seeded-growth method. And explanation of the principle of the "size focusing" growth, which leads to better size uniformity, (b) representative absorbance spectra of InAs QDs with the size tunability synthesized via the controlled injection of the amorphous nanocluster solution [64], and (c) the synthetic method and reaction scheme of InSb QDs using a seeded-growth method by continuously injecting clusters [67].

2.4 Others

Beyond the conventional synthesis methods discussed above, several emerging approaches recently have been developed. For example, the cation exchange replaced the original cations in the QDs lattice with the target cations in the

solution to achieve component transformation while maintaining the basic crystal morphology [70–72]. Shan *et al*. [73] utilized the high ion diffusivity of strongly ionic semiconductors, along with the facile formation of Cu vacancies, to synthesize wurtzite InAs NCs via the cation exchange reaction by using Cu_3As NCs as templates [Fig. 6(a)]. Another new method, the one-pot method, shared similar mechanisms with the hot-injection and heating-up, but the difference was that it further simplified the synthetic procedures and reduced the product loss and contamination risks associated with intermediate transfers. Sheikh *et al*. [55] presented a controlled one-pot synthesis strategy (using only readily available and less reactive precursors $InCl_3$ and AsI_3) to break through the wavelength limitation of InAs QDs to the SWIR region, achieving monodisperse InAs CNQDs with the bandgaps tunable from 1 200 nm to 1 800 nm [Fig. 6(b)]. Mir *et al*. [74] reported a facile one-pot synthesis strategy, in which the reaction was carried out by the in-situ formation of indium- and antimony-silylamide complex, which further formed covalently bonded indium and antimony triamide after reacting with oleylamine (OLA). This method balanced the reactivity of indium and antimony triamide with reducing agents, obtaining high-quality InSb QDs with stoichiometric composition [Fig. 6(c)]. By using size selection, the monodisperse InSb QDs were obtained with a size range from 4.2 nm±0.8 nm up to 8.5 nm±0.9 nm, and exhibited well-defined exciton transitions in the SWIR region of 1 250 nm–1 860 nm.

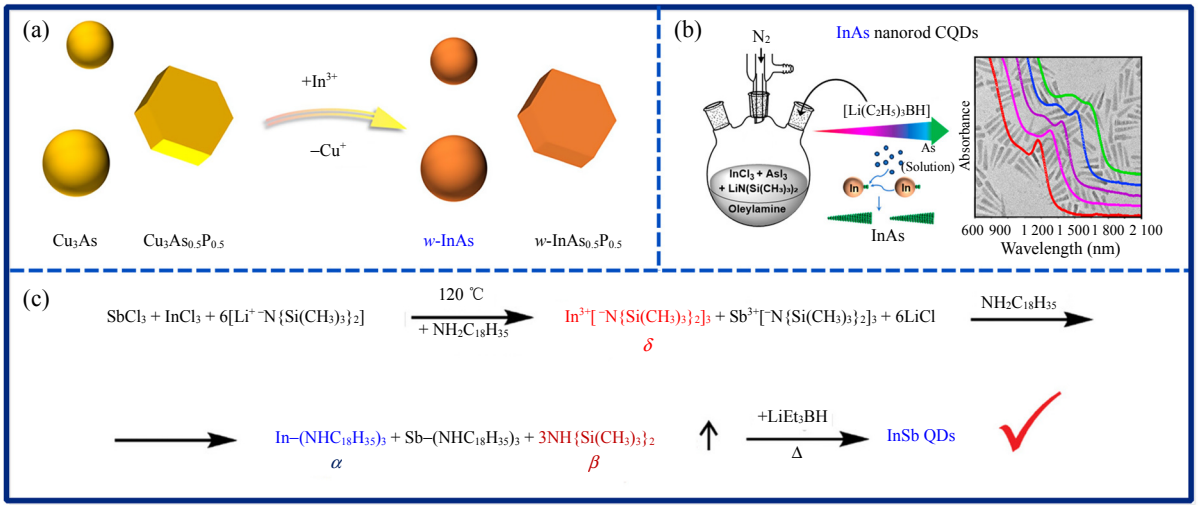


Fig. 6 Emerging synthetic routes to InX QDs via cation exchange and one-pot methods: (a) schematics of the synthesis of InAs NCs by cation-exchanging Cu_3As NCs with In [73], (b) the schematic depiction of the one-pot synthesis of monodisperse InAs CNQDs with the bandgaps tunable from ~1 200 nm to ~1 800 nm [55], and (c) the optimized reaction scheme used in the one-pot method for InSb QDs carried out by in-situ formation of indium- and antimony-silylamide complex [74].

2.5 Discussion and comparison

Currently, the synthesis methods for InX QDs primarily including hot-injection, heating-up, seeded growth, and cation exchange. Figure 7 offers a consolidated summary and systematic comparison of these representative methods, focusing on their critical advantages, disadvantages, and prospective applications. Given its analogous features to the heating-up approach, the one-pot method is not itemized separately in this comparison. Among these, the hot-injection method achieves enhanced monodispersity by separating the nucleation and growth stages. This technique manipulates reaction kinetics by altering parameters such as the precursor injection approaches (the single/dual-source and single/continuous injection), reaction temperature, synthesis time, or reducing agents, thereby enabling

the precise control of the size distribution of InX QDs. However, its temperature sensitivity makes this method unsuitable for the commercial-scale production. To address this limitation, the heating-up and seeded growth approaches have been developed as derivatives of the hot-injection. The heating-up method, characterized by pre-mixing reactants and subsequent co-heating, offers a simplified and reproducible pathway suitable for large-scale QDs synthesis, effectively circumventing the drawbacks inherent to the hot-injection. Nonetheless, there is still a certain gap in the monodispersity of InX QDs synthesized by the heating-up approach compared to the hot-injection method. According to the nucleation growth theory of the heating-up method, the optimal state of precursors is to remain the inert below the target temperature and rapidly transform into monomers when heated to the target temperature. Therefore, developing precursors or combinations of precursors and additives with temperature mutation characteristics in the future is one of the reference paths to address this limitation. Despite sacrificing some procedural convenience, the seeded growth method effectively mitigates the issue of the secondary nucleation encountered during prolonged high-temperature processing in both hot-injection and heating-up methods, establishing itself as the optimal route for producing large-sized InX QDs with superior monodispersity. Moreover, the seeded growth approach shows significant potential for morphology control, enabling the realization of complex geometries (e.g., tetrahedral and rod-like) via the directional epitaxial growth. It is noteworthy that other emerging synthetic pathways also possess distinct advantages. For instance, in cation exchange synthesis, residual metal ions can effectively passivate detrimental defect states, thereby enhancing the quality of the obtained InX QDs. The one-pot method combines the inherent benefits of the heating-up approach and eliminates additional precursor preparation steps. The reduction in synthesis steps minimizes the material loss and contact between reactants and the surrounding environment, effectively reducing the generation of oxygen/water induced defects in InX QDs.

In the future, the synthesis strategies of InX QDs will focus on integrating the advantages of diverse methods, aiming to establish a dynamic equilibrium among the precise size/morphology control, enhanced process simplicity/scalability, and reduced environmental impact. Such optimization is essential to meet the escalating demands of diverse applications for both superior material performance and commercial manufacturing.

Synthesis methods	Advantages	Disadvantages	Potential applications
Hot-injection	Excellent monodispersity High crystal quality	Scale-up challenges Stringent control requirements High process parameter sensitivity	Fundamental scientific research
Heating-up	Facile operation Ease of scale-up High reproducibility	Limited monodispersity	Industrial production
Seeded growth	Excellent monodispersity Core-shell structure construction Precise control	Process complexity Result uncertainty	Core-shell QD design Large-sized QD synthesis Morphology analysis of QDs
Cation exchange	Mild reaction condition Original morphology retention	Crystal defect formation Limited reaction uniformity	Novel multi-element QD synthesis

Fig. 7 Summary and comparison of current synthesis methods for InX QDs.

3. Performance optimization strategies of the InX QDs infrared photodetectors

Despite the successful synthesis of InX QDs exhibiting superior infrared optical properties through optimized synthetic methods and precursor selection, the construction of high-performance InX QDs infrared photodetectors confronts many problems at the materials and device levels, such as surface defects, low carrier mobility, inadequate infrared light absorption capacity, and limited carrier separation/transport efficiency within the devices [75–80]. As depicted in Fig. 8, this section systematically discusses diverse performance optimization strategies to address these multi-scale challenges in InX QDs-based infrared photodetectors.

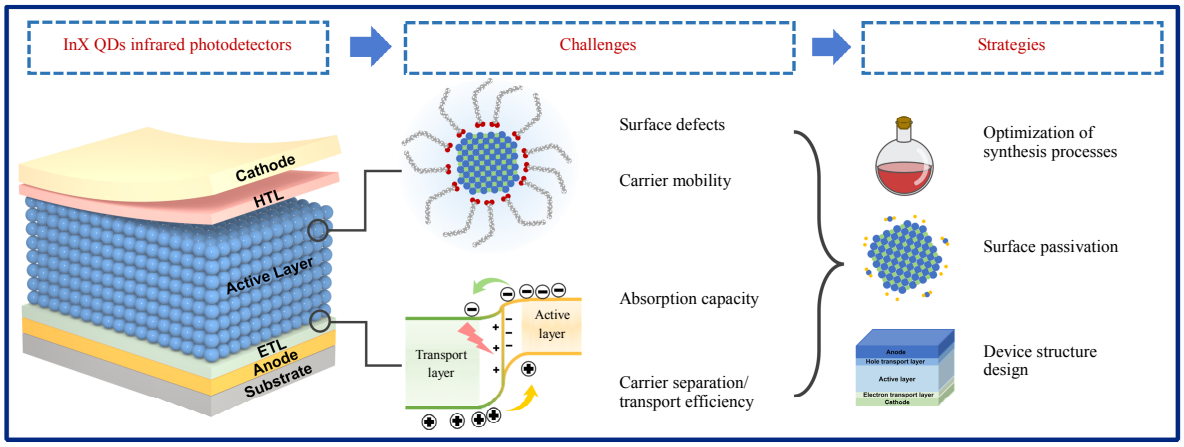


Fig. 8 Challenges and performance optimization strategies of the InX QDs infrared photodetector.

3.1 InAs QDs photodetectors

As shown in Table 1 [26, 54, 81–93], the InAs QDs infrared photodetectors have been developed rapidly in recent years, with different photoresponse mechanisms [mainly including the photoconductive (PC) effect and photovoltaic (PV) effect] emerging, and their photoelectric performances have been gradually improved. The improvement for the performance of the InAs QDs infrared photodetectors mainly starts from the following three aspects: 1) synthetic processes, 2) surface passivation, and 3) device structure design.

3.1.1 Optimization of the InAs QDs synthesis processes

InAs QDs, as photoactive materials, play a dominant role in the optoelectronic performance of InAs QDs photodetectors. In order to obtain high-performance photodetectors, it is crucial to optimize the InAs QDs synthesis process based on classical synthesis QDs techniques to obtain high-quality InAs QDs, such as the controllable and uniform size, monodispersity, high carrier mobility, and low defects. The monodisperse InAs QDs directly affect the optical and electrical properties and are crucial for high-performance InAs QDs infrared photodetectors. Although manifold methods for preparing InAs QDs based on different group-V arsenic precursors have been developed (primarily applied to luminescence), the InAs QDs demonstrating photoresponse in photodetectors have been mainly fabricated via either $(TMSi)_3As$ or $(TMGe)_3As$ precursors so far [94–96]. Sargent's research group [91] obtained monodisperse InAs QDs through surfactant treatment during the conventional QDs seeded growth synthesis process, which improved the photoelectric performances of InAs QDs infrared photodetectors. At the same time, the influence of two different precursors, $(TMSi)_3As$ and $(TMGe)_3As$, on the experimental results was compared. Figure 9(a) shows the schematic diagram

of the monodisperse InAs QDs synthesis using $(TMSi)_3As$ and $(TMGe)_3As$ precursors. Firstly, the InAs nanoclusters and seeds were synthesized separately, and then the InAs QDs were synthesized by continuously injecting InAs nanoclusters into InAs seeds. The results showed that the dioctylamine (DOA) played an important role in the synthesis of highly monodispersed InAs QDs. The DOA prevented rapid decomposition by forming a solvated shell around $(TMSi)_3As$, and its large steric hindrance made it close to indium atoms, thus slowing down the synthesis rate. The $(TMGe)_3As$-based InAs QDs exhibited more In-rich characteristics and a thicker amorphous In-oleate shell on the surface of QDs. As shown in Fig. 9(b), both the $(TMSi)_3As$- and $(TMGe)_3As$-based InAs QDs photodetectors have similar EQE values of 22% (0 V) and 28% (1 V) at 950 nm, confirming the successful synthetic route for two different precursors.

Table 1 Summary of InAs QDs infrared photodetectors.

Device structure	Photoresponse mechanism	Optimization strategy	Range (nm)	Responsivity (A/W)	Detectivity (Jones)	EQE (%)	Response/ recovery time	Ref.
ITO/ZnO/MaAc-$InBr_3$-InAs/MoO_x/Ag	PV	Surface passivation	950	0.283 at 0 V	1.9×10^{11}	37	1.0/1.4 μs	[26]
ITO/ZnO/InAs:Zn/MoO_3/Ag	PV	Synthetic processes + surface passivation	1 050	>0.1 at −0.5 V 1 mW/cm^2	2.98×10^{8}	–	–	[54]
ITO/ZnO/ME-InAs/MoO_3/Au	PV	Surface passivation	930	0.27 at 0 V	1.6×10^{11}	36	–/65 ns	[81]
ITO/ZnO/$InBr_3$-InAs/MoO_3/Au	PV	Surface passivation	940	0.22 at −1 V	1.0×10^{11}	37	2.3/2.0 ns	[82]
SiO_2/MCC-InAs/Al	PC	Surface passivation	–	–	–	–	–	[83]
ITO/ZnO NPs/ InAs/MTA-InAs /MoO_3/Ag	PV	Surface passivation+ device structure design	>1 000	0.3 at −1 V	–	35	–/1.5 μs	[84]
ITO/ZnO/InAs (ACN:DMF)/MoO_x/Au	PV	Device structure design	940	0.6 at −3 V	3.1×10^{11}	79	–/46 ns	[85]
SiO_2/ZnON/ME-InAs/ Ti/Al	PV+PC	Surface passivation+ device structure design	905	2.71×10^{4} at V_D −7 V 2×10^{-6} W/cm^2	5.02×10^{14}	5.23×10^{6}	2.90/3.44 μs	[86]
ITO/ZnO/$SnBr_2$-InAs/MoO_3/Au	PV	Surface passivation+ device structure design	1 020	0.36 at −1 V	1.63×10^{10}	43.1	19.7/21.2 μs	[87]
ITO/ZnO/InAs@ZnSe/ InAs/MoO_x/Au	PV	Surface passivation	1 450	0.17 at −1 V	1.2×10^{10}	14.9	–/~1 μs	[88]
ITO/ZnO/InAs(IPT)/ MoO_3/Au	PV	Surface passivation	920	2.167 at −5 V	1.9×10^{11}	292	12.4/36.1 ns	[89]
SiO_2/HCl-InAs/Al	PC	Surface passivation	980	5.45×10^{3} at V_D 50 V	1.74×10^{13}	6.9×10^{5}	–	[90]
ITO/ZnO/$InBr_3$-InAs/ MoO_3/Ag	PV	Synthetic processes+ surface passivation	950	–	4×10^{11} at −1 V	28	–/3.7 μs	[91]
ITO/ZnO NPs/Cl^--Br^-InAs /MoO_x/Ag	PV	Surface passivation	1 140	–	5×10^{11} at −1 V	75	–/10 ns	[92]
ITO/NiO/In(As,P)/ TiO_2:Nb/Al	PV	Synthetic processes+ device structure design	1 150	–	1.1×10^{10} at −4 V	5	1.2/0.6 μs	[93]

*ITO: indium tin oxide; ME: 2-mercaptoethanol; MCC: metal chalcogenide complexes; NPs: nanoparticles; MTA: methoxyacetic acid; ACN: acetonitrile; DMF: N,N-dimethylformamide; IPT: intermediate phase transfer.

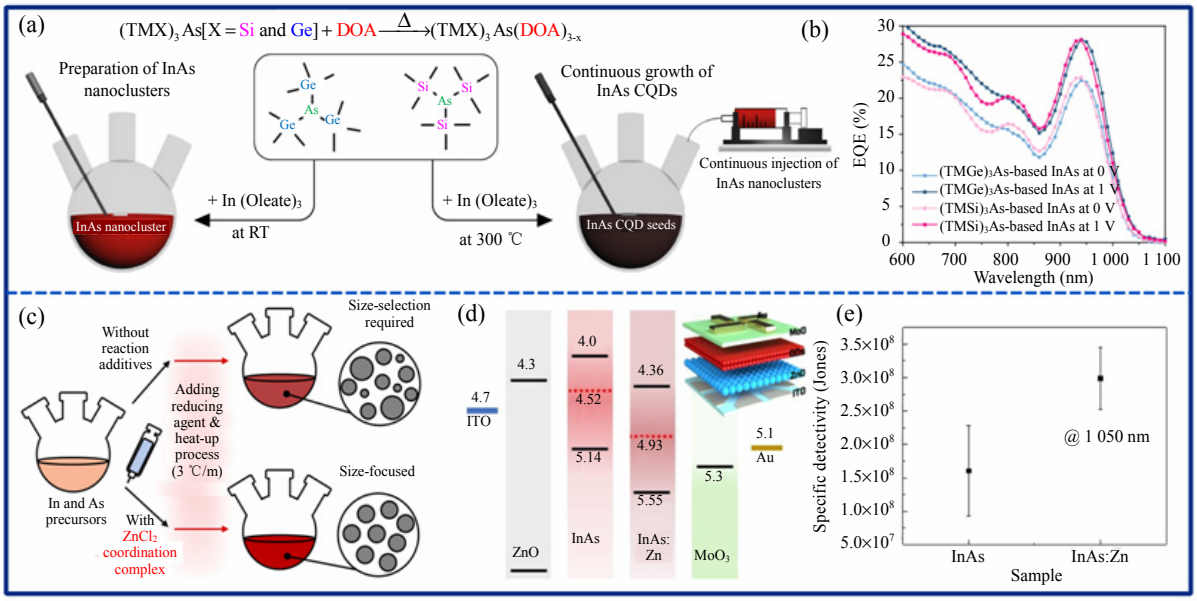


Fig. 9 Optimization strategy for the synthesis process toward monodisperse InAs QDs: (a) the schematic diagram of the monodisperse InAs QDs synthesis using $(TMSi)_3As$ and $(TMGe)_3As$ precursors, (b) the EQE of the different InAs QDs photodetectors at 0 V and 1 V [91], (c) the schematic diagram of the InAs QDs syntheses with and without the $ZnCl_2$-based coordination complex, (d) the energy band diagram and device structure diagram of the ITO/ZnO/InAs QDs/MoO_3/Au infrared photodiode, and (e) detectivities of the InAs and InAs:Zn QDs infrared photodiodes for 1 050 nm at 1 mW/cm^2 and 1 kHz [54].

Regarding the broad size distribution issue of the InAs QDs synthesized by the heating-up method using commercially available arsenic precursors, Kim *et al*. [54] introduced $ZnCl_2$-based reaction additives during the co-reduction process of indium and arsenic precursors and used zinc ions to passivate the surface of InAs QDs, reducing the size distribution and removing surface defects [Fig. 9(c)]. In addition, the Zn ions on the surface of InAs QDs modulated the energy level and carrier concentration, thus reducing the dark current and improving the optical response of the InAs:Zn QDs photodetector. Compared with InAs QDs, the InAs:Zn QDs showed a lower Fermi level (E_F), that was, the Zn ions had a p-type doping effect on InAs QDs. Although the optical response of the InAs:Zn QDs photodetector was not as large as that of the InAs QDs photodetector, the InAs:Zn QDs photodetector showed a lower dark current, so it showed a higher detectivity of $(2.98 \pm 0.46) \times 10^8$ Jones [Figs. 9(d) and 9(e)].

3.1.2 Surface passivation of the InAs QDs

Due to the high surface-to-volume ratio, there are some environmentally sensitive dangling bonds on the surface of InAs QDs, which are prone to forming defect centers. Furthermore, the original long-chain organic ligands result in long spatial distances between QDs, hindering charge transfer [97–100]. Suitable surface passivation can effectively address these problems and promote the application of InAs QDs in infrared photodetectors.

As a predominant surface passivation strategy, ligand exchange employs short-chain ligands to replace long-chain counterparts. This substitution passivates defects on the surface of QDs, thereby reducing the recombination probability of photogenerated carriers while concurrently enhancing charge carrier mobility. For InAs QDs, researchers have explored various ligands, such as molecular metal chalcogenide complexes (MCCs), thiol ligands, and metal halide ligands [83, 101, 102]. Sun *et al*. [82] reported an amphoteric $InBr_3$ passivator to reduce dangling bonds of InAs QDs for infrared photodetectors. As illustrated in Fig. 10(a), the $InBr_3$ can dissociate into X-type (Br^-) and Z-type ($InBr_2^+$) ligands efficiently passivating the In and As

dangling bonds on the surfaces, respectively. Compared to conventional OA-capped InAs QDs, the $InBr_3$-passivated InAs QDs exhibited distinct n-type transport characteristics, with energy level positions measured at −4.62 eV for the conduction band minimum (CBM), −5.92 eV for the valence band maximum (VBM), and −4.79 eV for E_F. In addition, this material showed a higher mobility-lifetime product, corresponding to a longer carrier diffusion length, reflecting an improved surface passivation [Fig. 10(b)]. Using InAs QDs passivated via this amphoteric dual passivation strategy, Sun *et al*. [82] designed a device architecture consisting of ITO/ZnO/InAs/MoO_3/Au. MoO_3 served as both a hole transport and an electron blocking layer in this photodetector, effectively suppressing the back injection of electrons and thus reducing dark current. Despite the existence of an energy level barrier at the ZnO/InAs interface, the device successfully achieved the zero bias operation, achieving an EQE of about 30% at 0 V, a D^* of 10^{11} Jones in the NIR region, and the rapid fall time of 2 ns, demonstrating typical high-performance photodiode characteristics. Future improvements in InAs QDs infrared device performance may rely on precise band alignment engineering through the advanced ligand design. Moreover, guided by the hard-soft acid-base theory, Jung *et al*. [87] found another amphoteric passivator $SnBr_2$. The high affinity of the hard-type $[SnBr]^+$ dissociated from $SnBr_2$ for the hard-type surface As atoms originated from its similar charge with the core In atoms and large adsorption energy. This drove the $[SnBr]^+$ ligand to migrate to an In site and formed bonds with three adjacent As atoms, resulting in a higher surface passivation density of InAs QDs. The InAs QDs treated with $SnBr_2$ exhibited a deeper EF compared to those treated with $SnCl_3$, resulting in a stronger built-in electric field at the interface with the ZnO electron transport layer (ETL). The optimized device achieved a higher open-circuit voltage, a maximum EQE of 43.1%, the responsivity of 0.36 A/W at 1 020 nm, and a faster response speed. Single-halide passivation became insufficient as the size of QDs increased. Xia *et al*. [92] devised a mixture halides passivation strategy targeting facet and edge exposure of the large InAs QDs, employing $InCl_3$ and $InBr_3$. Compared with individual halide (Cl^- or Br^-), the halide mixture exhibited significantly higher desorption energies on multiple QD facets, as well as at edges and vertex sites, leading to more complete and robust surface passivation. This enhanced surface integrity contributed to improving carrier mobility, reducing trap state density, and obtaining superior oxidation resistance. As a result, the photodetector achieved an exceptional EQE of 75% at 0.5 V with 10 ns rapid photoresponse.

Complementary to the direct exchange, the acid-mediated removal of surface oxides and native ligands has been attempted to facilitate subsequent passivation. Nevertheless, such treatment easily compromises the surface integrity of QDs and alters their optical characteristics. Shi *et al*. [89] designed a less invasive intermediate phase transfer (IPT) method for ligand exchange. As presented in Fig. 10(c), in the IPT process, the native OA ligands on InAs QD surfaces were first exchanged with aromatic organic ligands, enabling phase transfer into weakly polar solvents. The InAs QDs were then transferred into polar solvents, where a finely controlled surface reconstruction was mediated by thiol ligands, ultimately yielding stable QDs with enhanced electrical conductivity [89]. The polarization of the aromatic rings in the organic ligands played a critical role in maintaining colloidal stability of the QD ink in both weakly polar solvents and after secondary passivation in polar solvents. The InAs QDs infrared photodetector prepared by this method achieved a D^* of 1.9×10^{11} Jones at 0 V under 930 nm illumination, with the recovery time of 14 ns. In addition, the different ligand concentrations induced surface defect mediated light

proliferation, and the EQE of this device significantly increased to about 290% at −5 V, with the responsivity of 2.19 A/W, producing considerable gain effect (>10).

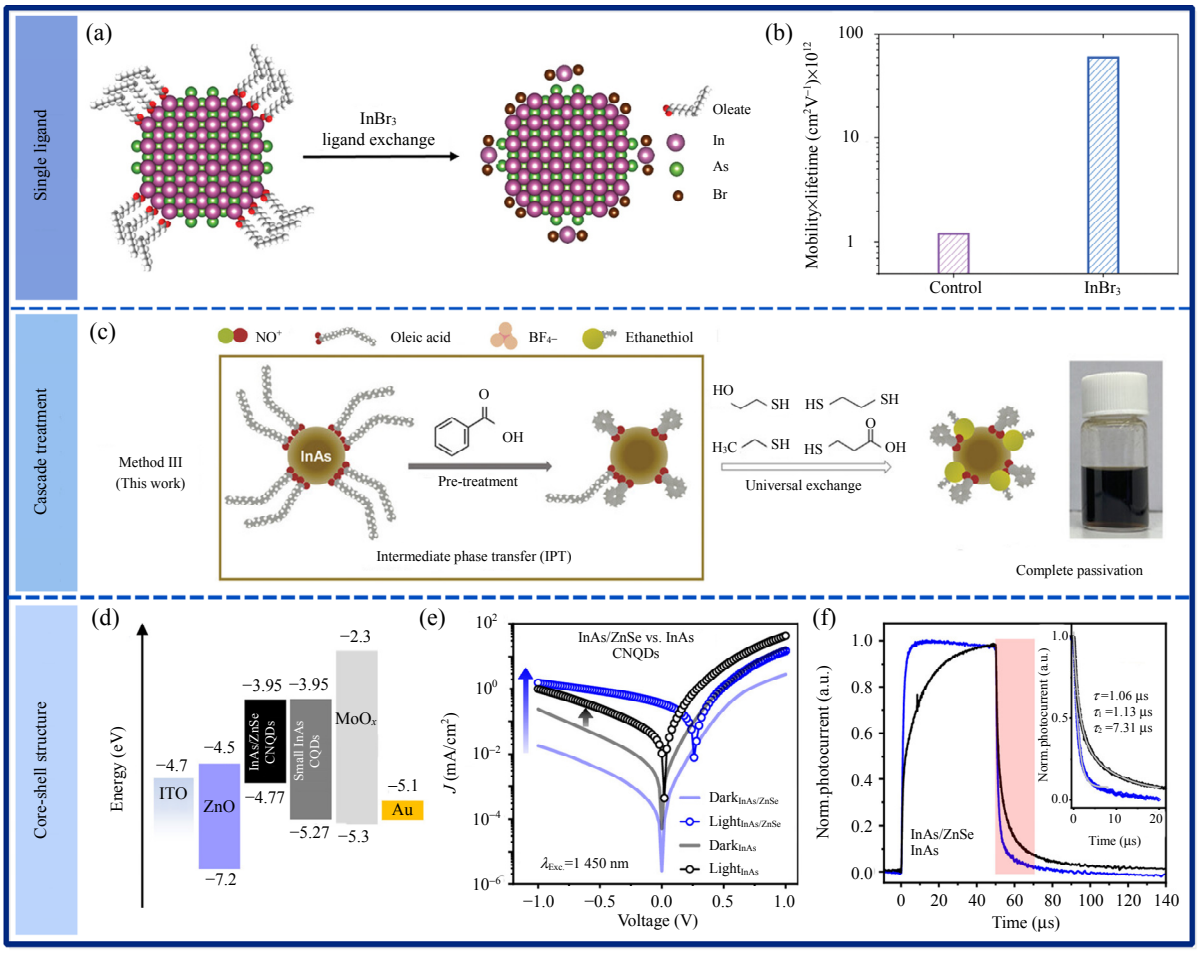


Fig. 10 Surface passivation strategy of InAs QDs: (a) the schematic diagram of the $InBr_3$ ligand exchange for InAs QDs stabilization, (b) the mobility-lifetime product of the InAs and $InBr_3$-InAs QDs films [82], (c) the schematic diagram of the ligand exchange using the IPT method for InAs CQDs and the optical photo of the InAs CQDs ink [89], (d) the band energy alignment diagram of the InAs/ZnSe CNQDs photodiode, (e) *J-V* plots of the InAs/ZnSe CNQDs photodiode and core-only photodiode under dark and 1 450 nm, and (f) transient photoresponse curves of the core-only InAs and InAs/ZnSe CNQDs photodiodes at 1 V, and the inset shows the fitting curves [88].

Alongside the ligand exchange, the core/shell structures can effectively passivate the surfaces of QDs, thus contributing to enhanced performance in photodetectors [103, 104]. Sheikh *et al.* [88] reported a two-step synthesis of the InAs/ZnSe core/shell CNQDs, featuring an ultrathin, uniform, and impurity-free ZnSe shell. The wide-bandgap ZnSe shell effectively passivated surface trap states while preserving charge transport efficiency, and served as a protective barrier between InAs CNQDs and the ambient atmosphere to prevent oxidation. The infrared photodetectors based on these CNQDs with the band structure depicted in Fig. 10(d) were fabricated. When illuminated by 1 450 nm, these heterostructure devices demonstrated significantly enhanced photoresponse compared to core-only InAs CNQD photodiodes, achieving a high EQE of 15%, D^* of 1.2×10^{10} Jones, and the reduced dark current density ($\sim10^{-2}$ mA/cm^2) as shown in Fig. 10(e). The surface passivation conferred by the core/shell architecture accelerated the response dynamics, yielding the fall time of 1 μs that represented a 7.3-fold improvement over core-only devices [~7.3 μs, Fig. 10(f)].

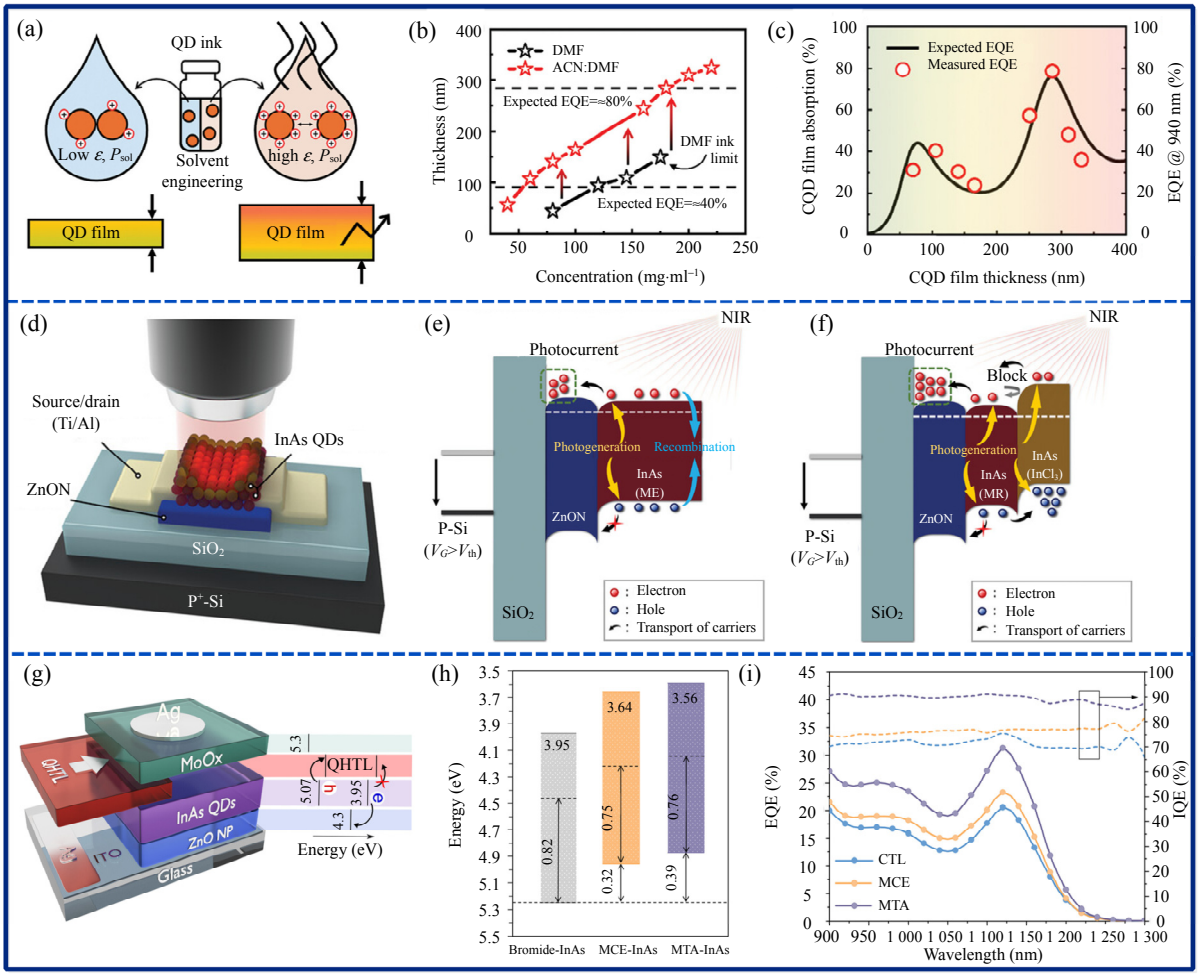


Fig. 11 Device structure design of InAs QDs photodetectors: (a) the schematic diagram of the ink solvent engineering strategy for the InAs QDs absorber layer, (b) the thicknesses of the different InAs QDs films, (c) the comparison of the maximum EQE values at 940 nm obtained according to the thickness of the InAs CQD PD absorber layer with the simulated absorption of the InAs CQD film [85], (d) the schematic diagram of the InAs QDs photodetector, carrier diffusion diagrams of the (e) ZnON/ME-InAs and (f) ZnON/ME-InAs/$InCl_3$-InAs [86], (g) the schematic diagram of the InAs QDs photodiode with the incorporation of a quantum-tuned hole transport layer with suitable energy levels, (h) the energy band diagram of the InAs QDs thin films after the indium bromide-based, MCE, and MTA ligand exchange, and (i) the EQE and estimated IQE of the different devices [84].

3.1.3 Device structure design of the InAs QDs photodetectors

In terms of the device structure, the photodetector performance hinges critically on the light absorption capability of the active layer and the efficiency of photogenerated carrier separation/transport [105, 106]. Through optical simulation analysis, Shin *et al*. [85] found that the limited EQE of the current InAs QDs infrared photodetectors could be partially attributed to insufficient light absorption caused by the thin thickness of the active layer. As shown in Fig. 11(a), they used a co-solvent strategy by mixing acetonitrile and N,N-Dimethylformamide (DMF) in a 2:1 volume ratio to increase the dielectric constant and vapor pressure, thereby extending the thickness of the InAs QD films. Figure 11(b) shows that the co-solvent system enabled the formation of thicker films at the same precursor concentration and allowed uniform film deposition over a wider thickness range (60 nm–330 nm), whereas films derived from the pure DMF tended to develop

cracks as the thickness increased. The increased film thickness enhanced light absorption and the series resistance while suppressing leakage pathways, which resulted in a lower dark current of the InAs QD photodetector. As shown in Fig. 11(c), the thickness-dependent trend of the EQE is in good agreement with the predicted value of the optical simulation. By this simple solvent engineering, the performance of the InAs QD photodetector achieved an over three-fold improvement in D^* from 9.8×10^{10} Jones (at the 105 nm thickness) to 3.1×10^{11} Jones (at the 290 nm thickness), and a high EQE of 79% at 940 nm wavelength. In addition, as the film thickness increased, the reduction in resistor-capacitor time was greater than the increase in the carrier transport time, resulting in a decreasing trend in the response time (the minimum value can reach 43 ns).

The performance of pure QDs-based photodetectors is often limited by the inherently low carrier mobility and high surface defect density of QDs, which result in a short carrier diffusion length in films. A promising strategy to break this performance bottleneck involves constructing structures by combining QDs with novel materials [e.g., 2-dimensional (2D) materials, other QDs, organic semiconductors, or perovskites] to form hybrid active layers with hetero-/homojunctions or matched charge transport layers. This strategy enhances the separation and extraction efficiency of photogenerated carriers, thereby improving device performance. Particularly, the integration of 2D materials and QDs creates a highly complementary system. While 2D materials offer extraordinary carrier mobility, their ultrathin nature limits light absorption. Conversely, QDs feature high absorption coefficients, effectively compensating for this weakness. Shim *et al*. [107] demonstrated a WS_2/InAs QDs phototransistor, which achieved a high responsivity of 1.134 A/W over a wide infrared range (>1 000 nm) and exhibited a synaptic behavior. The performance stemmed from a designed type-II heterojunction. The tunability of the bandgap and work function in WS_2 (by the layer number) and InAs QDs (by the size) facilitated optimal band alignment. The weak p-type behavior of pristine WSe_2 (from substrate dangling bonds and Se vacancies) and the ligand-induced n-type character of InAs QDs created a strong intrinsic electric field at the interface. This enhanced the carrier separation and transfer, yielding the detection performance superior to that of either material alone. In addition, Kim *et al*. [86] engineered an amorphous metal oxide semiconductor phototransistor integrated with the ligand-modified InAs QDs, with the device architecture detailed in Fig. 11(d). InAs QDs coated with mercaptoethanol (ME) and $InCl_3$ ligands were sequentially deposited on zinc oxynitride (ZnON) to form an infrared absorption layer with the gradated bandgap structure. The values of E_F of ZnON, ME-InAs, and $InCl_2$-InAs were located at −3.88 eV, −3.89 eV, and −4.02 eV, respectively, while their VBM lay at −5.35 eV, −4.99 eV, and −4.86 eV, respectively. When the gate voltage exceeded the threshold voltage, the E_F of each layer shifted upward in the direction opposite to the gate bias, thereby reducing the potential barrier height and turning the device into the on state [Fig. 11(e)]. Photogenerated holes and electrons behaved differently and electrons were readily transferred to the ZnON layer, whereas holes were hindered by the valence band barrier at the ZnON/ME-InAs interface. The captured holes would recombine in the InAs QD layer and induce electron recycling in the ZnON layer. The built-in electric field formed by the ME-InAs/$InCl_3$-InAs QDs homojunction structure [Fig. 11(f)] effectively separated photogenerated holes and electrons, and suppressed carrier recombination. Compared to the ZnON/ME-InAs device, this structure enhanced the detection performance by accelerating the electron recycling process in the ZnON layer, achieving the

maximum responsivity exceeding 10^5 A/W and D^* exceeding 10^{16} Jones in the NIR region.

Suitable transport layers can prevent carrier backflow and minimize recombination losses, thus reducing the leakage current of photodetectors. Currently, InX QDs face challenges in achieving proper rectification and efficient junctions due to band-edge offsets and poor energy level alignment with conventional transport layers. Vafaie *et al*. [84] mitigated the poor rectification and elevated dark current density associated with MoO_x by introducing an intervening hole transport layer (HTL) with a shallow energy level between MoO_x and the InAs QD layers. The overall upward shift of the energy levels in HTLs facilitated the hole extraction and electron blockage. Once transported to this new interlayer, holes were injected into the MoO_x layer via interface trap-assisted tunneling [Fig. 11(g)]. InAs QDs with a first excitonic absorption peak at 900 nm were selected as the HTL material. These QDs were further modified with 2-mercaptoethanol (MCE) and methoxyacetic acid (MTA) ligands, enabling the comparative performance evaluation of infrared photodetectors based on these two distinct InAs QDs-based hole transport layers. After treatment with MCE and MTA liagnds, the energy levels of InAs QDs shifted upward [Fig. 11(h)], significantly raising the CBM and resulting in a shallower VBM (MCE-InAs QDs: 4.95 eV and MTA-InAs QDs: 4.88 eV). Compared to the MCE ligand, the carboxylate groups of the MTA ligand could interact with multiple active surface centers through bridging bidentate coordination, enabling more stable passivation. This configuration more effectively reduced the defect density in quantum dots while improving electrical conductivity and carrier lifetime. Due to the good surface passivation and matched energy level structure design, the MTA-InAs device achieved a higher peak EQE of 35% at 1 450 nm and a lower dark current density of 400 nA/cm² [Fig. 11(i)]. And Siddik *et al*. [108] introduced copper(I) iodide (CuI) with a deeper VBM and back-end-of-line compatible amorphous indium gallium zinc oxide (a-IGZO) as charge transport layers to form a CuI-InAs QD-IGZO PIN heterojunction that promoted efficient carrier separation and full depletion. The optimized device achieved a dark current density of 4.7 μA/cm^2 at −1 V and an EQE of 25% at 1 210 nm. Furthermore, this design incorporated a complementary metal oxide silicon (CMOS)-compatible TiN bottom electrode, and the pixelated photodiode array was further integrated with a CMOS readout integrated circuit (ROIC), enabling infrared imaging using a 512×768-pixel array for the first time.

3.2 InSb QDs photodetectors

Although the InAs QDs-based infrared photodetectors exhibit the excellent detection performance in the NIR band, the device performance deteriorates when the wavelength extends beyond 1 200 nm/1 300 nm. Given that expanding the detection range to the SWIR region (above 1 400 nm) is crucial for eye safe applications and improving target recognition capabilities, there is an urgent need to develop high-performance photodetectors that cover this wavelength range [109, 110]. Notably, utilizing the large-sized InAs QDs to access longer wavelengths poses significant challenges due to the extremely stringent synthesis and optimization requirements. In contrast, the InSb QDs exhibit significant advantages in achieving efficient SWIR photodetection (Table 2), [46, 53, 57–59, 67, 69, 111–113] due to their inherent material properties. Based on these, this section focuses on the InSb QDs infrared photodetectors, systematically reviews the research progress in recent years, and discusses from three key dimensions: the synthesis process optimization, surface passivation strategy, and device structure design.

Table 2 Summary of InSb QDs infrared photodetectors.

Device structure	Photoresponse mechanism	Optimization strategy	Range (nm)	Responsivity (A/W)	Detectivity (Jones)	EQE (%)	Response/ recovery time	Ref.
Si/SiO_2/InSb: PCBM:Poly-TPD/Ag	PV	Device structure design	1 400	0.000 4 at 1.35 W/cm^2	1.5×10^6	0.155	80/80 ms	[46]
Au/Na_2S-InSb/Au	PC	Surface passivation	1 350	–	–	0.8	–/5 s	[53]
ITO/ZnO/Zn:InSb/ MoO_x/Ag	PV	Synthetic processes+ surface passivation	1 380	0.35 at 1 V 10.4 mW/cm^2	1×10^{12}	33	–/1.4 μs	[57]
ITO/ZnO/TABX-MAX-InSb/MoO_3/Au	PV	Synthetic processes+ surface passivation	1 200	>0.7 at −1 V	1.0×10^{11}	75	7.3/5.4 μs	[58]
ITO/ZnO/MA-TBAI-InSb/MoO_x/Ag	PV	Synthetic processes+ surface passivation	1 400	0.28 at −1 V	1.4×10^{11}	25	–/5.6 μs	[59]
ITO/ZnO/$InBr_3$-InSb: $InBr_3$-InAs/MoO_3/Au	PV	Device structure design	1 550	0.003 76 at 0.867 W/cm^2	2.7×10^8	–	112/206 ms	[67]
ITO/ZnO/InSb/ Spiro-OMeTAD/ MoO_3/Au	PV	Synthetic processes+ surface passivation	1 520	0.057 at 0 V 32 mW/cm^2	3.07×10^{12}	4.64	–	[69]
ITO/TiO_2/InSb@InP/ MoO_x/Au	PV	Surface passivation+ device structure design	1 240	–	4.4×10^{11} at 0 V	5 at 2 V	68/70 ns	[111]
TO/PEDOT:PSS/InSb/ ZnO/Al	PV	Surface passivation	1 100	0.18 at −1 V 1 mW/cm^2	–	18.52	–/0.2 s at 0 V	[112]
ITO/PEDOT:PSS/ $InBr_3$-InSb/ZnO/Al	PV	Surface passivation	1 200	0.098 at −1 V 1 mW/cm^2	–	10.1	0.55/0.8 s	[113]

*ITO: indium tin oxide; PEDOT:PSS: poly(3,4-ethylenedioxythiophene):poly(styrenesulfonate); PCBM: [6,6]-phenyl C_{61}-butyric acid methyl ester; Poly-TPD: polymeric triphenyldiamine (poly(N,N'-diphenylben-zidine diphenylether); TABX-MAX-InSb: InSb QDs treated with a mixture of tetrabutylammonium halides and methylammonium halides; MA: malonic acid; TBAI: tetrabutylammonium iodide; Spiro-OMeTAD: 2,2',7,7'-Tetrakis(N,N-di-p-methoxyphenylamine)-9,9'-spirobifluorene.

3.2.1 Optimization of the InSb QDs synthesis process

Similar to InAs QDs, the monodispersity of InSb QDs also greatly governs the performance of their infrared photodetectors. Prof. Sargent's group [58] achieved excellent control over the size distribution of InSb QDs by introducing additional metal halides during synthesis. Zinc halide formed a stable adduct with the N,N-dimethylethylamine (DMEDA) reducing agent, limiting the interaction with the antimony precursor, and thereby adjusting the reduction rate. The InSb QDs obtained via this method exhibited widely tunable exciton absorption peaks across 960 nm–1 270 nm and steep absorption edges without long tails, which was a hallmark of highly monodisperse QDs ensembles. After the ligand exchange, the InSb QDs infrared photodetector was demonstrated for the first time, achieving a D^* of 1.02×10^{11} Jones and a record-setting EQE of 75% at 1 200 nm for heavy-metal-free infrared devices. Afterwards, they optimized the synthesis parameters and used organic additives to further regulate the reactivity of the indium precursor, which differed from previous work that only used the OLA as the coordination solvent for precursors [57]. As shown in Fig. 12(a),

in the co-existing environment of the OLA and trioctylphosphine (TOP)/trioctylamine (TOA)/ triphenylphosphine (TPP), the indium preferentially complexed with the TOP/TOA, while the TPP was inhibited from complexing with $InCl_3$ due to its larger steric hindrance, and antimony preferentially formed stable adducts with the OLA. At the required temperature, the organic additives subsequently released precursors in a controllable manner to obtain highly monodisperse InSb QDs, whose absorption spectrum was extended to 1 500 nm and the peak-to-valley ratio reached 1.5. Leveraging these optimized InSb QDs, an infrared photodiode with an ITO/ZnO/InSb QDs/MoO_x/Ag architecture was designed, attaining the specific detectivity of 10^{12} Jones and an EQE of 33% at 1 380 nm. The device still maintained 90% of its initial performance after 19 h of continuous illumination. As shown in Fig. 12(b), these values contribute to the highest EQE and operational stability for III-V QDs-based devices operating in the same wavelength range of 1 300 nm–1 500 nm.

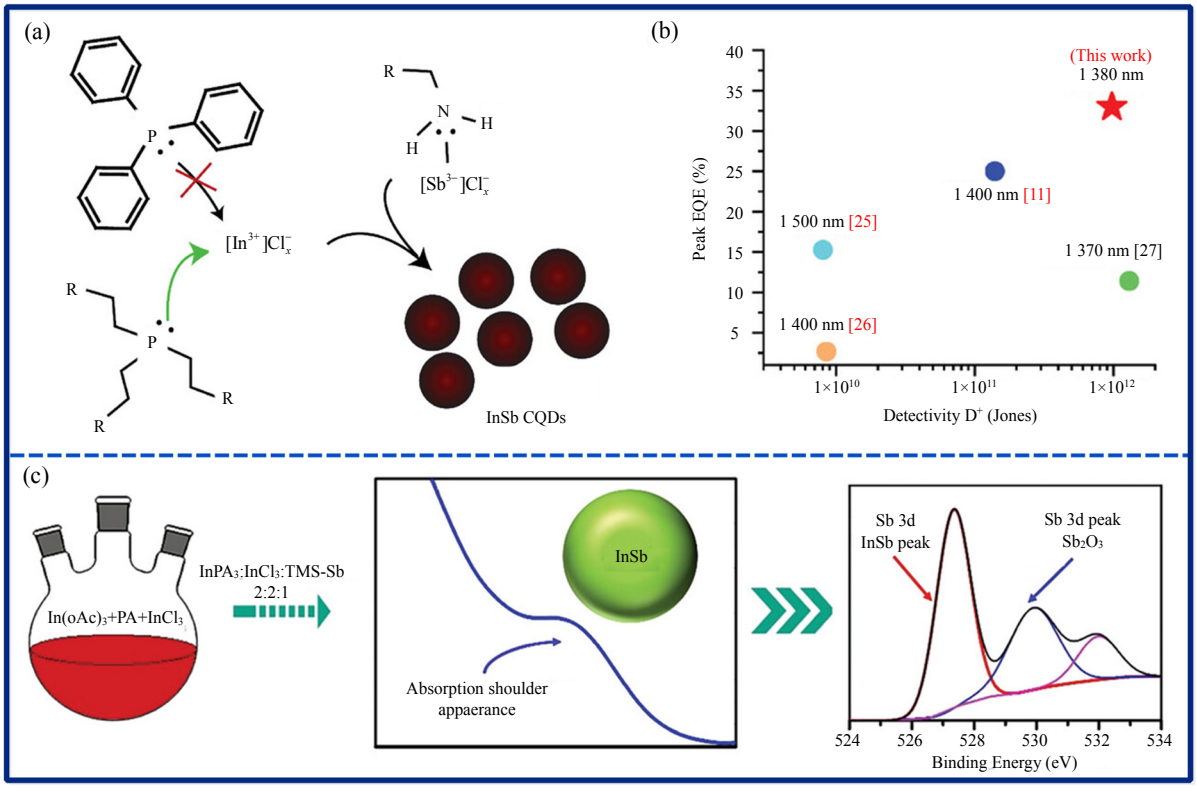


Fig. 12 Reaction kinetics modulation strategy enabling monodisperse InSb QDs for high-performance infrared photodetection: (a) the schematic diagram of the reactivity mechanism between phosphines and $InCl_3$, (b) the comparison of the device performance with previous III-V QDs-based photodetectors [57], and (c) InSb QDs properties depending on precursors (schematic illustration, absorption spectrum, and XPS peak fitting results) [69].

Beyond the challenge of the size distribution control, the pronounced oxygen affinity of InSb presents a significant obstacle, rendering the QDs highly susceptible to oxidation during both synthesis and post-synthetic processing. For larger InSb QDs, this fragility becomes particularly critical because InSb QDs have an easily oxidizable indium rich surface. To address oxidation during the InSb synthesis, Seo *et al*. [69] employed a mixture indium precursor of $InCl_3$-TOP and $In(OAc)_3$, alongside $(TMS)_3Sb$. The InSb QDs prepared solely with $In(OAc)_3$ lacked discernible absorption shoulders, while those from composite precursors displayed pronounced shoulder peaks. The X-ray

photoelectron spectroscopy (XPS) analysis revealed the disappearance of the O 1s peak and the reduction in the Sb_2O_3 peak for the $InPA_3$-$InCl_3$ [Fig. 12(c)]. This suppression of oxidation was attributed to the surface passivation effect of the Cl^- ligands. They constructed a photodetector featuring an ITO/ZnO/InSb QDs/Spiro-OMeTAD/MoO_3/Au architecture, demonstrating superior performances of J_D (3.3×10^{-9} A/cm^2), R (0.126 A/W), and D^* (3.9×10^{12} Jones) at 1 370 nm; J_D (1.5×10^{-9} A/cm), R (0.078 A/W), and D^* (3.6×10^{12} Jones) at 1 520 nm at 0 V bias.

3.2.2 Surface passivation of the InSb QDs

As one of the conventional surface passivation strategies for InSb QDs, the ligand exchange effectively optimizes the optoelectronic characteristics by adjusting the surface charge balance, shortening particle spacing, improving the carrier mobility, and reducing the defect density. Typical ligands used include MCC, $InBr_3$, and Na_2S [53, 113].

Chatterjee *et al*. [112] mixed the OLA-capped InSb QDs dissolved in n-octane with a formamide (FA) solution of Na_2S. As the liquid-phase ligand exchange was completed, the InSb QDs were completely transferred from the n-octane phase (top layer) to the FA phase (bottom layer) [Fig. 13(a)]. The grazing-incidence small-angle X-ray diffraction (GI-XRD) patterns of the OLA-, sulfide- and bromide-capped InSb QDs are shown in Fig. 13(b). The diffraction peak of the OLA-capped QDs occurred at 2θ=0.85°, whereas the diffraction peaks were shifted to 2θ=0.98° and 1.2° for the bromide- and sulfide-capped counterparts. The calculation showed that the interparticle distance of the InSb QDs decreased from 11 nm to 7.5 nm. The peak broadened as the peak-to-valley ratio decreased, suggesting an increase in the packing density of InSb QDs and proving successful ligand exchange. Figure 13(c) shows the large difference in the zeta potential, where the steric repulsion on the surface for sulfide-capped InSb QDs was much weaker than that of the bromide-capped counterpart, which also confirmed the difference in the dispersion behaviors of InSb QDs observed by GI-XRD. Critically, sulfide-terminated InSb QDs exhibited the significantly enhanced carrier mobility along with an elevation of the highest occupied molecular orbital and lowest unoccupied molecular orbital (HOMO-LUMO) energy levels. This ultimately reduced the energy barrier between the photoactive layer and the PEDOT:PSS HTL, resulting in a more favorable band alignment. The improved energy structure increased the built-in potential and promoted more efficient carrier transport while suppressing the dark current. The sulfide-capped InSb QDs photodiode demonstrated a low dark current (~nA/cm^2) and the 18.5% EQE at 1 100 nm with the response time of 5.5 ms.

Owing to the inherent oxophilicity, large surface-to-volume ratio, and detrimental dangling bonds, the InSb QDs are prone to oxidation when exposed to an air environment, forming stable insulating indium/antimony oxide on the surface. To achieve efficient charge transfer between QDs, Zhang *et al*. [59] proposed a cascade ligand exchange strategy. The process began with etching the surface of InSb QDs by the mild MA which could remove the In and Sb oxides maintaining the integrity of QDs [Fig. 13(d)]. In addition, the two carboxyl groups of the MA could coordinate with metal atoms in a bidentate bridging mode, thus establishing a preliminary passivation. The process was followed by halide passivation with the TBAI, resulting in final products that exhibited the n-type behavior. Compared to traditional one-step halide passivation methods, it was more advantageous because the acid etching step created a cleaner surface and allowed a higher ligand coverage in subsequent exchange steps. The InSb QDs treated with the cascade exchange strategy showed the trap density reduction of 1.1×10^{16} cm^{-3} [Fig. 13(e)] and

an electron mobility increase of 3–4 times [Fig. 13(f)], demonstrating better electronic coupling. The obtained photodetector had an EQE of 25% at 1 400 nm with a bias voltage of 1 V, a detection rate of 1.4×10^{11} Jones, and the response time of 5.6 μs. Apart from acids (acetic acid and MA), the intermediate ligands of thiols can also play the same role. Imran *et al*. [57] used alkylthiol to reconstruct the InSb QDs surface. The thiols effectively removed surface oxides and loosely bound excess Z-type $InCl_3$ by donating protons to hydroxyl groups, thereby releasing oleylammonium chloride and enabling the binding of thiolate species to surface indium atoms. And the InSb QDs photodiode fabricated with this additional processing step exhibited a significantly enhanced performance, achieving an EQE of 33% at 1 380 nm with the specific detectivity of 10^{12} Jones, along with the improved operational stability [57].

The ligand exchange offers immediate surface passivation, and its transient stability under thermal/optical stress and sufficiency under the high surface defect density require more robust solutions. Core/shell heterostructures have become a viable alternative. Peng *et al*. [111] passivated the surface trap states of InSb QDs by developing an InP shell structure and successfully fabricated a SWIR photodetector based on these well passivated InSb/InP core-shell QDs [Fig. 13(g)]. It exhibited competitive features, including a wide linear dynamic range exceeding 128 dB, a maximum EQE of 25% at 1 240 nm (12% at 1 420 nm), the fast response time of 70 ns, and the specific detectivity of up to 4.4×10^{11} Jones at 1 400 nm [Figs. 13(h) and 13(i)].

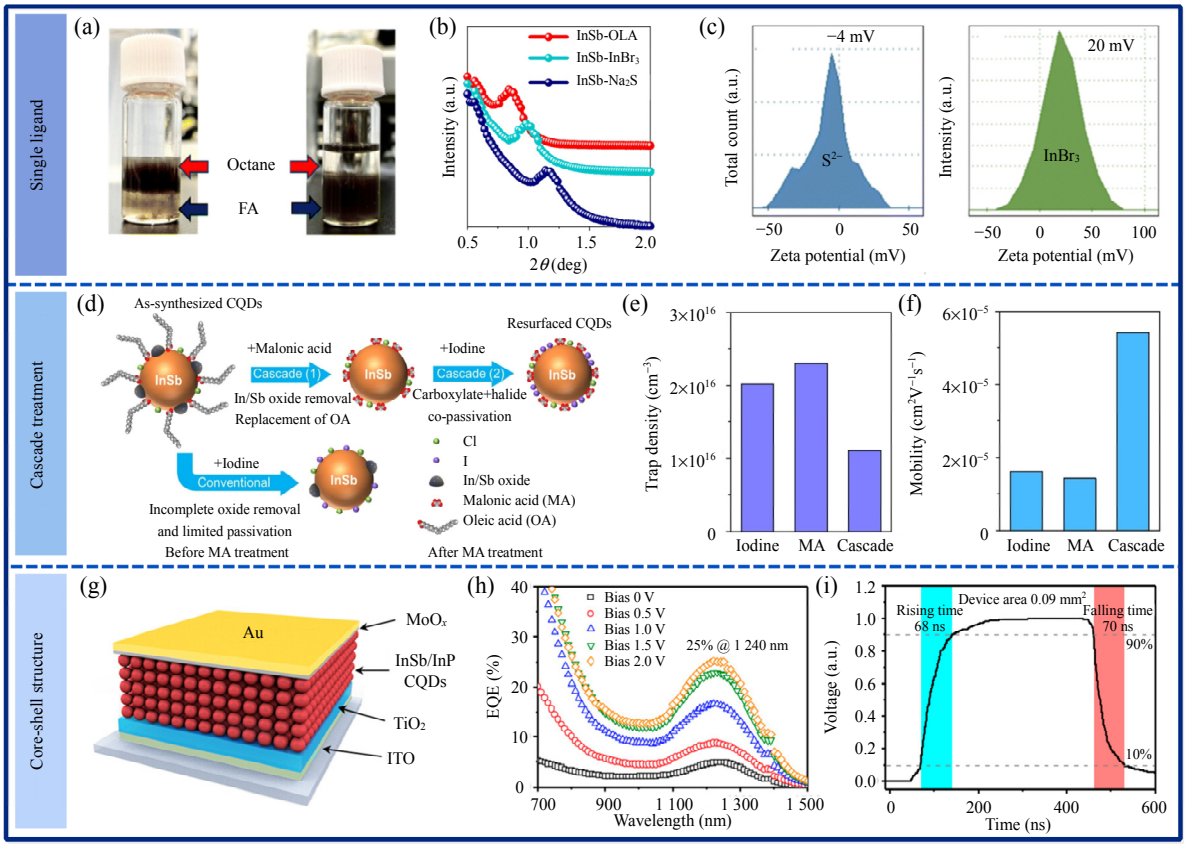


Fig. 13 Surface engineering strategy of InSb QDs: (a) photographs of the phase change before and after sulfide ligand exchange, (b) the low-angle GIXRD of the InSb QDs with OLA- and sulfide-capped ligands, (c) Zeta potentials of the InSb QDs capped with sulfide and bromide ligands [112], (d) the schematic diagram of the cascade ligand exchange in comparison with the one-step halide exchange, the comparison of (e) trap densities and (f) the carrier mobility extracted from the space-charge limited current [59], (g) the schematic diagram of the InSb/InP QDs photodetector, (h) the EQE of the InSb/InP QDs photodetector biased from 0 V to 2 V (reverse bias), and (i) the response time of the InSb/InP QDs photodetector [111].

Although Seo *et al*. [69] also reported InSb/InAs core/shell architectures, this structure exhibited a slightly lower result than the only-core device. The degradation was attributable to enhanced exciton recombination resulting from the type-I band alignment. Consequently, the core/shell passivation strategies demanded meticulous material selection to circumvent performance losses induced by the lattice mismatch, band offset disparities, and carrier transport barriers.

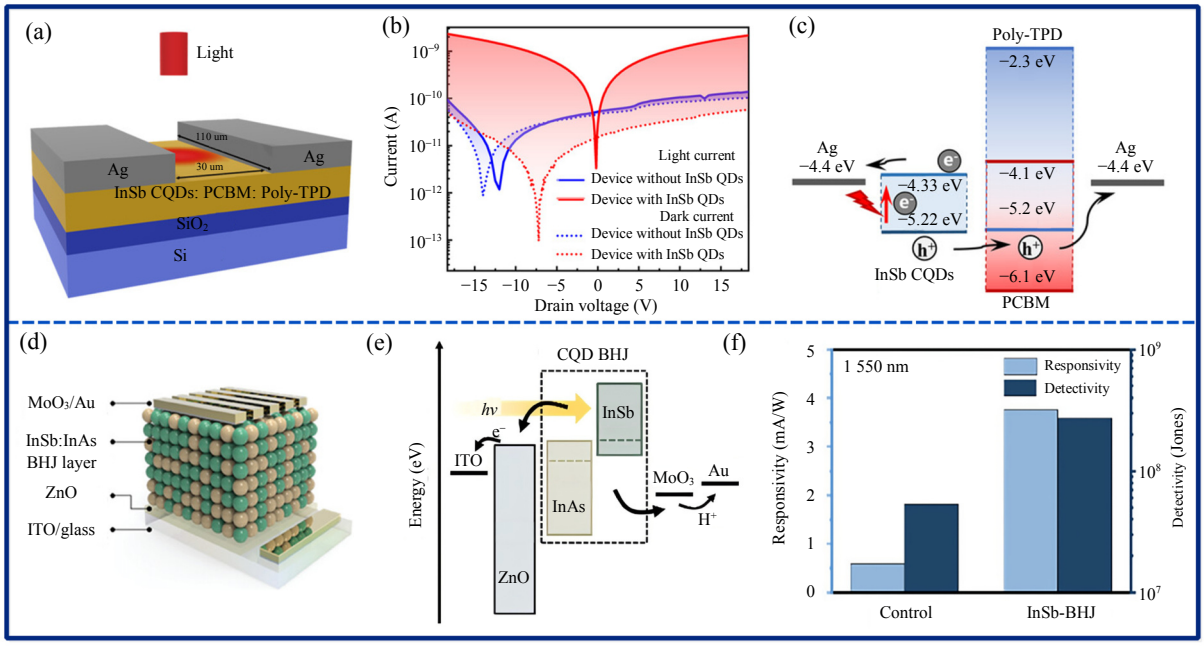


Fig. 14 Device structure design of InSb QDs photodetectors: (a) the schematic diagram of the InSb QDs:PCBM:poly-TPD photodetector, (b) *I-V* curves of the device with and without InSb QDs, (c) the schematic energy levels diagram of the photodetector under light excitation [46], (d) the schematic diagram of the InSb QDs photodiode, (e) the operation mechanism diagram of the InSb QDs photodiode, and (f) the comparison of responsivity and detectivity with the InSb photodiode and BHJ structure [67].

3.2.3 Device structure design of the InSb QDs photodetectors

Constructing heterojunction active layers through different materials integration also represent a critical approach for enhancing infrared photodetectors based on InSb QDs. Organic semiconductors show the significant potential for photodetector applications due to the low cost, simple fabrication, and high flexibility. Furthermore, they can form favorable heterojunctions with QDs, which can facilitate the dissociation and transport of photogenerated excitons. He *et al*. [46] pioneered the NIR photodetection capability in InSb QD devices by formulating a transistor active layer comprising OLA-capped InSb QDs blended with the organic small molecule PCBM and polymer Poly-TPD [Fig. 14(a)]. As evidenced by the *I-V* curves in Fig. 14(b), the pure InSb QDs photodetector exhibited negligible photoresponse due to high potential barriers at InSb QDs/metal electrode interfaces. Conversely, the hybrid device demonstrated a significantly enhanced performance that relied on the optimized band alignment [Fig. 14(c)]. The shallow VBM of Poly-TPD and the deep CBM of the PCBM facilitated the photogenerated carrier separation/transport across the ternary hybrid interpenetrating networks and efficient charge collection at Ag electrodes. The detection range of the hybrid device could cover 1 400 nm with the peak responsivity and specific detectivity reaching 0.4 mA/W and 1.5×10^6 Jones, respectively. Simultaneously, the deep lowest unoccupied molecular orbital level of the Poly-TPD and the shallow highest occupied molecular orbital

level of the PCBM established energy barriers that suppressed the reverse carrier transport, effectively minimizing the leakage current and ultimately yielding the reduced dark current density. Furthermore, Jee *et al*. [67] engineered a photodiode incorporating an InSb:InAs QDs bulk-heterojunction (BHJ) active layer [Fig. 14(d)]. The n-type InAs QDs and p-type InSb QDs formed a type-II heterojunction to facilitate the charge transfer, where large-bandgap InAs QDs only played as a transport pathway [Fig. 14(e)]. The resulting InSb:InAs QDs device showed a detectivity improvement of 2.7×10^8 Jones at 1 550 nm, which was twice as high as that of the control InSb device [Fig. 14(f)].

To achieve improved energy level alignment, Peng *et al*. [111] introduced TiO_2 to replace the conventional transport layer ZnO, which resulted in the enhanced rectification behavior while mitigating the carrier trapping effect associated with ZnO. This strategy significantly enhanced the fast response capability of photodetectors to meet imaging requirements. This InSb QDs device not only improved the detection performance (EQE/D^*), but also increased the response speed to the nanosecond order.

4. Conclusions and perspective

In this review, we summarized and discussed the research progress of InX QDs infrared photodetectors from the following two aspects: 1) common synthesis methods of InX QDs (the hot-injection, heating-up, seeded-growth, etc.); 2) performance optimization strategies of the InX QDs infrared photodetectors (the synthesis process optimization, surface passivation, and device structure design). However, opportunities and challenges coexist, and the prospects of InX QDs infrared photodetectors are as follows:

1) Synthesis process optimization: currently, the synthesis process based on InX QDs is still in the development stage, and achieving controllable preparation of InX QDs with good monodispersity faces significant challenges. Existing synthesis methods typically rely on size screening steps to obtain narrow size distributions that meet basic requirements. The development of more stable and safe precursors and reducing agents has become a crucial step in promoting its transformation from academic research to commercial applications. In addition, the current synthesis methods also have the problem of mismatched reaction rates between reducing agents and precursors, which can easily lead to an increase in by-products. Finding appropriate additives to precisely regulate nucleation growth kinetics is expected to address these problems and achieve well monodisperse InX QDs synthesis.

2) Device performance improvement: although the currently reported InX QDs have good infrared optical properties, the conversion from materials to devices is limited by multiple factors. In addition to the influence of monodispersity, the surface passivation, charge transfer efficiency, film uniformity, and energy level matching between various functional layers of the device all affect the performances of the InX QDs-based infrared photodetectors. In response to the above challenges, the collaborative optimizations are needed from the following dimensions:

a) Surface engineering innovation: considering the oxygen affinity of InX QDs, existing ligand engineering techniques (typically used for PbS QDs) may not be the optimal solution. The synergistic passivation strategy using the weak acid combined with multiple ligands can more effectively remove surface oxides of InX QDs, facilitate more sufficient binding of subsequent ligands, achieve surface defect state suppression and quantum dot spacing reduction, thereby improving carrier mobility and reducing the probability of non-radiative recombination in the photosensitive layer.

b) Doping modification: doping is also an effective strategy for adjusting the energy level structure and charge carrier dynamics of InX QDs.

The embedding of impurity atoms can regulate the concentration of charge carriers, change the E_F position, form localized states within the bandgap, optimize the distribution of carrier concentration, and enhance the charge transport efficiency and interface injection dynamics.

c) Heterogeneous structure design: while the performance of devices based on InX QDs is often constrained by their inherent surface defects and low carrier mobility, their excellent infrared absorption capability offers a significant advantage. Forming complementary heterostructures with other classes of materials can compensate for this limitation. For instance, the high mobility of 2D materials can facilitate the charge transport, the passivation effect of perovskites can mitigate surface defects, and the plasmonic enhancement of metal nanoparticles can boost light harvesting. By integrating these distinct properties, such heterostructures are expected to overcome the bottlenecks of single-material systems and substantially enhance the photodetection performance of InX QDs-based devices.

d) Transport layer optimization: optimizing the electron/hole transport layer can effectively address the serious carrier recombination at the interface of the device functional layer caused by the energy level mismatch between it and the InX QDs active layer.

3) Large scale preparation and expanding applications: due to the heavy-metal-free composition and significant infrared photodetection capability, the InX QDs photodetectors demonstrate the substantial potential in photonic communications, imaging systems, and biomedical sensing. The potential implementation includes logic gates, high-resolution infrared imaging systems, wearable night-vision devices, and industrial gas leak detection. However, current research remains predominantly focusing on the single device level, and only a few studies on InAs QDs have advanced on the monolithic integration of pixel arrays. Addressing the challenge of scalable fabrication and integration is paramount for unlocking practical applications and commercial viability. Continued innovation in the synthesis, ligand engineering, and device design is essential to improve the performance and stability, drive forward large-scale production, and ultimately achieve the complete replacement of heavy-metal-based infrared photodetectors.

Acknowledgment

This work is supported by the National Natural Science Fund for Distinguished Young Scholars (Grant No. 62225106), National Natural Science Foundation of China (Grant No. U24A20229), and Sichuan Innovation Research Group Project (Grant No. 2025NSFTD0008).

Declarations

Conflict of Interest Huiling TAI is an editorial board member for Photonic Sensors and was not involved in the editorial review, or the decision to publish this article. All authors declare that there are no competing interests.

Permissions All the included figures, tables, or text passages that have already been published elsewhere have obtained the permission from the copyright owner(s) for both the print and online format.

Open Access This article is distributed under the terms of the Creative Commons Attribution 4.0 International License (http://creativecommons.org/licenses/by/4.0/), which permits unrestricted use, distribution, and reproduction in any medium, provided you give appropriate credit to the original author(s) and the source, provide a link to the Creative Commons license, and indicate if changes were made.

Use of AI Statement None.

References

[1] W. Zeng, Z. Duan, Y. Bu, H. Yu, C. Wang, X. Tang, *et al.*, "A self-powered HgTe quantum dots/PBDB-T:Y6 bipolar broadband photodetector for logic gates," *Materials Horizons*, 2025, 12(7): 2179–2186.

[2] W. Zeng, Z. Duan, Y. Bu, H. Yu, C. Wang, X. Tang, *et al.*, "Advances in bipolar photodetectors: working principles, constructions, and applications," *Laser & Photonics Reviews*, 2025, 19(8): 2402163.

[3] J. Yang, Z. Duan, W. Zeng, Y. Bu, X. Tang, G. Wang,

et al., "Two-step ligand exchange to promote charge transfer in PbSe quantum dot photodetectors for pulse monitoring," *Nanoscale Horizons*, 2025, 10(11): 2841–2849.

[4] Z. Li, Z. He, C. Xi, F. Zhang, L. Huang, Y. Yu, *et al*., "Review on III-V semiconductor nanowire array infrared photodetectors," *Advanced Materials Technologies*, 2023, 8(13): 2202126.

[5] A. R. Benasco, C. T. Liu, B. Rax, G. Mariani, S. McClure, T. Bills, *et al*., "Radiation hardened infrared photodetectors based on a narrow bandgap conjugated polymer semiconductor," *Advanced Electronic Materials*, 2025, 11(11): 2400918.

[6] M. I. Saleem, A. K. K. Kyaw, and J. Hur, "Infrared photodetectors: recent advances and challenges toward innovation for image sensing applications," *Advanced Optical Materials*, 2024, 12(33): 2401625.

[7] J. M. Hartmann, A. Abbadie, A. M. Papon, P. Holliger, G. Rolland, T. Billon, *et al*., "Reduced pressure-chemical vapor deposition of Ge thick layers on Si (001) for 1.3–1.55 μm photodetection," *Journal of Applied Physics*, 2004, 95(10): 5905–5913.

[8] J. Zha, M. Luo, M. Ye, T. Ahmed, X. Yu, D. H. Lien, *et al*., "Infrared photodetectors based on 2D materials and nanophotonics," *Advanced Functional Materials*, 2022, 32(15): 2111970.

[9] P. Zhang, Y. Sun, J. Sun, S. Wang, R. Wang, and J. Zhang, "Progress in 2D material-based infrared photodetectors for intelligent vision applications," *Advanced Functional Materials*, 2025, 35(36): 2502072.

[10] M. Amani, C. Tan, G. Zhang, C. Zhao, J. Bullock, X. Song, *et al*., "Solution-synthesized high-mobility tellurium nanoflakes for short-wave infrared photodetectors," *ACS Nano*, 2018, 12(7): 7253–7263.

[11] M. Long, A. Gao, P. Wang, H. Xia, C. Ott, C. Pan, *et al*., "Room temperature high-detectivity mid-infrared photodetectors based on black arsenic phosphorus," *Science Advances*, 2017, 3(6): e1700589.

[12] Y. Bu, Y. Jiang, Z. Duan, W. Zeng, X. Tang, J. Yang, *et al*., "Oriented crystallization of HgTe quantum dots with low urbach band-tail for broadband optoelectronic logic gates," *Advanced Optical Materials*, 2025, 13(19): 2500295.

[13] S. Zhan, B. Li, T. Chen, Y. Tu, H. Ji, D. M. Othman, *et al*., "High responsivity colloidal quantum dots phototransistors for low-dose near-infrared photodetection and image communication," *Light: Science & Applications*, 2025, 14(1): 201.

[14] X. Tang, Y. Jiang, Z. Duan, Y. Bu, W. Zeng, J. Yang, *et al*., "Surface ligand engineering of Ag_2Te colloidal quantum dots for a self-powered shortwave infrared photodetector," *Journal of Materials Chemistry C*, 2025, 13(42): 21418–21427.

[15] X. Zhang, G. Mu, Y. Zhang, Y. Jiang, and Y. Yan, "Heavy metal-free colloidal quantum dots: preparation and application in infrared photodetectors," *Journal of Materials Chemistry C*, 2024, 12(39): 15811–15832.

[16] Q. Li, J. Li, H. Chen, W. Zhang, S. Cao, F. Chu, *et al*. "The enhancement of infrared characterization of passivated InAs nanowires," *Micro and Nanostructures*, 2024, 191: 207867.

[17] R. Xu, Y. Sun, Y. Zhu, F. Wang, J. Wang, L. Cheng, *et al*., "Tunable surface band bending enables switchable photoconductance of colloidal InSb nanowires for self-powered and broadband photodetectors with fast response," *Applied Surface Science*, 2024, 670: 160690.

[18] A. A. Guzelian, U. Banin, A. V. Kadavanich, X. Peng, and A. P. Alivisatos, "Colloidal chemical synthesis and characterization of InAs nanocrystal quantum dots," *Applied Physics Letters*, 1996, 69(10): 1432–1434.

[19] H. B. Jalali, S. Sadeghi, M. Sahin, H. Ozturk, C. W. Ow-Yang, and S. Nizamoglu, "Colloidal aluminum antimonide quantum dots," *Chemistry of Materials*, 2019, 31(13): 4743–4747.

[20] S. W. Kim, J. P. Zimmer, S. Ohnishi, J. B. Tracy, J. V. Frangioni, and M. G. Bawendi, "Engineering $InAs_xP_{1-x}$/InP/ZnSe III-V alloyed core/shell quantum dots for the near-infrared," *Journal of the American Chemical Society*, 2005, 127(30): 10526–10532.

[21] D. K. Harris and M. G. Bawendi, "Improved precursor chemistry for the synthesis of III-V quantum dots," *Journal of the American Chemical Society*, 2012, 134(50): 20211–20213.

[22] D. Battaglia and X. Peng, "Formation of high quality InP and InAs nanocrystals in a noncoordinating solvent," *Nano Letters*, 2002, 2(9): 1027–1030.

[23] Y. Zhang, M. Imran, P. Xia, Y. Chen, A. Gulsaran, Y. Liu, *et al*., "Nucleophilic covalent ligands enable simultaneous surface reconstruction and passivation of colloidal InSb quantum dots for stable short-wave infrared photodetectors," *Angewandte Chemie International Edition*, 2025, 64(28): e202505179.

[24] M. S. Skorotetcky, W. J. Mir, T. Sheikh, K. E. Yorov, B. M. Saidzhonov, S. Daws, *et al*., "Si-H hydrosilane reducing agents for size-and shape-controlled InAs colloidal quantum dots," *Advanced Materials*, 2025, 37(4): 2412105.

[25] Q. Wang, C. Sun, Z. Liu, B. Zeng, Y. Chen, Z. Liu, *et al*., "Stepwise crystallization synthetic strategy for monodisperse InSb colloidal quantum dots with mid-infrared absorption," *Angewandte Chemie International Edition*, 2025, 64(25): e202506387.

[26] P. Xia, B. Sun, M. Biondi, J. Xu, O. Atan, M. Imran, *et al*., "Sequential co-passivation in InAs colloidal quantum dot solids enables efficient near-infrared photodetectors," *Advanced Materials*, 2023, 35(28): 2301842.

[27] Y. Y. Pan, J. L. Pan, Y. K. Wang, and L. S. Liao, "III-V quantum dots: a multidimensional exploration from eco-friendly materials to near infrared optoelectronic applications," *Materials Today*, 2025, 85: 172−188.
[28] Y. Huang, Q. Hou, J. Kong, K. Wang, L. Huang, Z. Du, *et al*., "Advances in defect modulation strategies of indium antimonide semiconductor colloidal quantum dots for infrared photodetection," *Journal of Materials Chemistry A*, 2025, 13(10): 7055−7072.
[29] C. Hu, A. I. Channa, L. Xia, X. Li, Z. Li, Z. M. Wang, *et al*., "Colloidal InAs quantum dots: synthesis, properties, and optoelectronic devices," *Advanced Functional Materials*, 2025, 35(32): 2500280.
[30] H. Xie, C. Zhang, R. Yang, J. Xu, Y. Pan, and X. Yin, "From synthesis to application in infrared photodetectors: a review of InSb colloidal quantum dots," *Laser & Photonics Reviews*, 2025, 19(4): 2401204.
[31] J. Seo, S. Kim, D. Yeo, N. Gwak, and N. Oh, "Pnictide-based colloidal quantum dots for infrared sensing applications," *Nano Convergence*, 2025, 12(1): 26.
[32] A. Soosaimanickam, P. Manidurai, S. Krishna Sundaram, and M. B. Sridharan, "*Advancements and challenges in synthesizing colloidal semiconductor nanocrystals by hot-injection method*," in Nanomaterials: The Building Blocks of Modern Technology: Synthesis, Properties and Applications, T. Khan, M. Jawaid, K. A. Ahmad, and B. Singh, Eds., Singapore: Springer Nature, 2023: 143–179.
[33] V. K. LaMer and R. H. Dinegar, "Theory, production and mechanism of formation of monodispersed hydrosols," *Journal of the American Chemical Society*, 1950, 72(11): 4847–4854.
[34] D. Franke, D. K. Harris, L. Xie, K. F. Jensen, and M. G. Bawendi, "The unexpected influence of precursor conversion rate in the synthesis of III-V quantum dots," *Angewandte Chemie*, 2015, 127(48): 14507−14511.
[35] D. Franke, D. K. Harris, O. Chen, O. T. Bruns, J. A. Carr, M. W. B. Wilson, *et al*., "Continuous injection synthesis of indium arsenide quantum dots emissive in the short-wavelength infrared," *Nature Communications*, 2016, 7(1): 12749.
[36] J. Zhang and D. Zhang, "Photoluminescence and growth kinetics of high-quality indium arsenide and InAs-based core/shell colloidal nanocrystals synthesized using arsine (AsH_3) generated via zinc arsenide as the arsenic source," *Chemistry of Materials*, 2010, 22(4): 1579−1584.
[37] V. Grigel, D. Dupont, K. De Nolf, Z. Hens, and M. D. Tessier, "InAs colloidal quantum dots synthesis via aminopnictogen precursor chemistry," *Journal of the American Chemical Society*, 2016, 138(41): 13485−13488.
[38] V. Srivastava, E. Dunietz, V. Kamysbayev, J. S. Anderson, and D. V. Talapin, "Monodisperse InAs quantum dots from aminoarsine precursors: understanding the role of reducing agent," *Chemistry of Materials*, 2018, 30(11): 3623−3627.
[39] C. M. Evans, S. L. Castro, J. J. Worman, and R. P. Raffaelle, "Synthesis and use of tris(trimethylsilyl)antimony for the preparation of InSb quantum dots," *Chemistry of Materials*, 2008, 20(18): 5727−5730.
[40] A. Maurice, M. L. Haro, B. Hyot, and P. Reiss, "Synthesis of colloidal indium antimonide nanocrystals using stibine," *Particle & Particle Systems Characterization*, 2013, 30(10): 828–831.
[41] M. Yarema and M. V. Kovalenko, "Colloidal synthesis of InSb nanocrystals with controlled polymorphism using indium and antimony amides," *Chemistry of Materials*, 2013, 25(9): 1788−1792.
[42] S. Tamang, K. Kim, H. Choi, Y. Kim, and S. Jeong, "Synthesis of colloidal InSb nanocrystals via in situ activation of $InCl_3$," *Dalton Transactions*, 2015, 44(38): 16923−16928.
[43] S. Busatto, M. D. Ruiter, J. T. B. H. Jastrzebski, W. Albrecht, V. Pinchetti, *et al*., "Luminescent colloidal InSb quantum dots from in situ generated single-source precursor," *ACS Nano*, 2020, 14(10): 13146−13160.
[44] L. Peng, Y. Wang, C. Rodà, A. Malla, M. Dosil, D. Mandal, *et al*., "Suppressing colloidal quantum dot multimer fusion leads to high-performance InSb infrared photodetectors," *Advanced Science*, 2025, 12(27): 2502775.
[45] Y. Kwon, O. Yeromina, M. Cavallo, M. G. Silly, D. Pierucci, E. Lhuillier, *et al*., "Synthesis of NIR/SWIR absorbing InSb nanocrystals using indium(I) halide and aminostibine precursors," *Advanced Functional Materials*, 2024, 34(40): 2403912.
[46] M. He, Z. Xu, S. W. Zhang, M. Zhang, C. Wu, B. Li, *et al*., "Colloidal InSb quantum dots/organic integrated bulk heterojunction for fast and sensitive near-infrared photodetectors," *Advanced Photonics Research*, 2022, 3(4): 2100305.
[47] S. G. Kwon and T. Hyeon, "Formation mechanisms of uniform nanocrystals via hot-injection and heat-up methods," *Small*, 2011, 7(19): 2685–2702.
[48] J. Van Embden, A. S. R. Chesman, and J. J. Jasieniak, "The heat-up synthesis of colloidal nanocrystals," *Chemistry of Materials*, 2015, 27(7): 2246–2285.
[49] J. Park, A. Jayaraman, X. Wang, J. Zhao, and H. S. Han, "Nanocrystal precursor incorporating separated reaction mechanisms for nucleation and growth to unleash the potential of heat-up synthesis," *ACS Nano*, 2020, 14(9): 11579–11593.
[50] R. L. Wells, C. G. Pitt, A. T. McPhail, A. P. Purdy, S.

Shafieezad, and R. B. Hallock, "The use of tris (trimethylsilyl)arsine to prepare gallium arsenide and indium arsenide," *Chemistry of Materials*, 1989, 1(1): 4–6.

[51] R. L. Wells, S. R. Aubuchon, S. S. Kher, M. S. Lube, and P. S. White, "Synthesis of nanocrystalline indium arsenide and indium phosphide from indium(III) halides and tris(trimethylsilyl)pnicogens. synthesis, characterization, and decomposition behavior of $I_3InP(SiMe_3)_3$," *Chemistry of Materials*, 1995, 7(4): 793–800.

[52] A. Das, A. Shamirian, and P. T. Snee, "Arsenic silylamide: an effective precursor for arsenide semiconductor nanocrystal synthesis," *Chemistry of Materials*, 2016, 28(11): 4058–4064.

[53] T. Zhao, N. Oh, D. Jishkariani, M. Zhang, H. Wang, N. Li, *et al*., "General synthetic route to high-quality colloidal III-V semiconductor quantum dots based on pnictogen chlorides," *Journal of the American Chemical Society*, 2019, 141(38): 15145–15152.

[54] S. Kim, S. Yeon, M. Lee, J. Jin, S. Shin, N. Gwak, *et al*., "Chemically and electronically active metal ions on InAs quantum dots for infrared detectors," *NPG Asia Materials*, 2023, 15(1): 30.

[55] T. Sheikh, W. J. Mir, S. Nematulloev, P. Maity, K. E. Yorov, M. N. Hedhili, *et al*., "InAs nanorod colloidal quantum dots with tunable bandgaps deep into the short-wave infrared," *ACS Nano*, 2023, 17(22): 23094–23102.

[56] W. Liu, A. Y. Chang, R. D. Schaller, and D. V. Talapin, "Colloidal InSb nanocrystals," *Journal of the American Chemical Society*, 2012, 134(50): 20258–20261.

[57] M. Imran, D. B. Kim, P. Xia, F. Y. Villanueva, B. Rehl, J. M. Pina, *et al*., "Control over metal-halide reactivity enables uniform growth of InSb colloidal quantum dots for enhanced SWIR light detection," *Advanced Materials*, 2025, 37(12): 2420273.

[58] Muhammad, D. Choi, D. H. Parmar, B. Rehl, Y. Zhang, O. Atan, *et al*., "Halide-driven synthetic control of InSb colloidal quantum dots enables short-wave infrared photodetectors," *Advanced Materials*, 2023, 35(46): 2306147.

[59] Y. Zhang, P. Xia, B. Rehl, D. H. Parmar, D. Choi, M. Imran, *et al*., "Dicarboxylic acid-assisted surface oxide removal and passivation of indium antimonide colloidal quantum dots for short-wave infrared photodetectors," *Angewandte Chemie*, 2024, 136(8): e202316733.

[60] B. Chen, D. Li, and F. Wang, "InP quantum dots: synthesis and lighting applications," *Small*, 2020, 16(32): 2002454.

[61] J. Ning and U. Banin, "Magic size InP and InAs clusters: synthesis, characterization and shell growth," *Chemical Communications*, 2017, 53(17): 2626–2629.

[62] S. F. Sandeno, S. M. Krajewski, R. A. Beck, W. Kaminsky, X. Li, and B. M. Cossairt, "Synthesis and single crystal X-ray diffraction structure of an indium arsenide nanocluster," *ACS Central Science*, 2024, 10(3): 744–751.

[63] J. Shin, M. Choi, D. Shim, T. J. Ziehl, S. Park, E. Cho, *et al*., "Unveiling the nanocluster conversion pathway for highly monodisperse InAs colloidal quantum dots," *JACS Au*, 2024, 4(3): 1097–1106.

[64] S. Tamang, S. Lee, H. Choi, and S. Jeong, "Tuning size and size distribution of colloidal InAs nanocrystals via continuous supply of prenucleation clusters on nanocrystal seeds," *Chemistry of Materials*, 2016, 28(22): 8119–8122.

[65] J. H. Song, H. Choi, H. T. Pham, and S. Jeong, "Energy level tuned indium arsenide colloidal quantum dot films for efficient photovoltaics," *Nature Communications*, 2018, 9(1): 4267.

[66] T. Kim, S. Park, and S. Jeong, "Diffusion dynamics controlled colloidal synthesis of highly monodisperse InAs nanocrystals," *Nature Communications*, 2021, 12(1): 3013.

[67] S. Jee, M. J. Si, J. H. Choi, D. Kim, C. Kim, D. Yang, *et al*., "P-type colloidal InSb quantum dot ink enables III-V group bulk-heterojunction shortwave infrared (SWIR) photodetector," *Advanced Optical Materials*, 2024, 12(18): 2303097.

[68] L. K. Sagar, G. Bappi, A. Johnston, B. Chen, P. Todorović, L. Levina, *et al*., "Single-precursor intermediate shelling enables bright, narrow line width InAs/InZnP-based QD emitters," *Chemistry of Materials*, 2020, 32(7): 2919–2925.

[69] H. Seo, H. J. Eun, A. Y. Lee, H. K. Lee, J. H. Kim, and S. W. Kim, "Colloidal InSb quantum dots for 1 500 nm SWIR photodetector with antioxidation of surface," *Advanced Science*, 2024, 11(4): 2306439.

[70] J. L. Stein, M. I. Steimle, M. W. Terban, A. Petrone, S. J. L. Billinge, X. Li, *et al*., "Cation exchange induced transformation of InP magic-sized clusters," *Chemistry of Materials*, 2017, 29(18): 7984–7992.

[71] J. Yang, F. Münzer, W. Baek, R. Fainblat, H. Chang, G. Bacher, *et al*., "Chemical synthesis, doping, and transformation of magic-sized semiconductor alloy nanoclusters," *Journal of the American Chemical Society*, 2017, 139(19): 6761–6770.

[72] B. J. Beberwyck and A. P. Alivisatos, "Ion exchange synthesis of III-V nanocrystals," *Journal of the American Chemical Society*, 2012, 134: 19977−19980

[73] X. Shan, Y. Zhou, B. Li, Z. Zeng, and B. Ji, "Wurtzite InAs nanocrystals with short-wavelength infrared emission synthesized through the cation exchange of Cu_3As nanocrystals," *Chemistry of Materials*, 2023, 35(6): 2569−2578.

[74] W. J. Mir, T. Sheikh, S. Nematulloev, P. Maity, K. E. Yorov, A. H. Emwas, *et al*., "One-pot colloidal

synthesis enables highly tunable InSb short-wave infrared quantum dots exhibiting carrier multiplication," *Small*, 2024, 20(19): 2306535.
[75] X. Li, Z. Yang, Z. Liang, P. Luan, N. Chen, X. Li, *et al*., "Optimizing thin films and device structures for the design of PbS colloidal quantum dots near-infrared photodetectors," *ACS Applied Electronic Materials*, 2024, 6(6): 4257–4268.
[76] T. Jia, Y. Hong, Z. Wei, B. Mu, and X. Yu, "Two-step ligand-exchange-assisted charge transfer in graphene/PbS quantum dots hybrid near-infrared photodetector," *ACS Applied Electronic Materials*, 2024, 6(3): 2066–2074.
[77] Y. Wang, M. Chen, M. Hu, A. Jiao, F. Wang, X. Zheng, *et al*., "A hybrid-ligand exchange strategy for high-performance PbSe quantum dot short-wave infrared photodetectors," *Journal of Materials Chemistry C*, 2025, 13(30): 15547–15554.
[78] K. Xu, L. Ke, H. Dou, R. Xu, W. Zhou, Q. Wei, *et al*., "Large photomultiplication by charge-self-trapping for high-response quantum dot infrared photodetectors," *ACS Applied Materials & Interfaces*, 2022, 14(12): 14783–14790.
[79] T. Mano, A. Ohtake, and T. Kuroda, "Lattice-mismatched epitaxy of InAs on (111)A-oriented substrate: metamorphic layer growth and self-assembly of quantum dots," *Physica Status Solidi A*, 2023, 221(13): 2300767.
[80] U. Bothra, M. Albaladejo-Siguan, Y. Vaynzof, and D. Kabra, "Impact of ligands on the performance of PbS quantum dot visible-near-infrared photodetectors," *Advanced Optical Materials*, 2023, 11(1): 2201897.
[81] M. J. Choi, L. K. Sagar, B. Sun, M. Biondi, S. Lee, A. M. Najjariyan, *et al*., "Ligand exchange at a covalent surface enables balanced stoichiometry in III-V colloidal quantum dots," *Nano letters*, 2021, 21(14): 6057–6063.
[82] B. Sun, A. M. Najarian, L. K. Sagar, M. Biondi, M. J. Choi, X. Li, *et al*., "Fast near-infrared photodetection using III-V colloidal quantum dots," *Advanced Materials*, 2022, 34(33): 2203039.
[83] W. Liu, J. S. Lee, and D. V. Talapin, "III-V nanocrystals capped with molecular metal chalcogenide ligands: high electron mobility and ambipolar photoresponse," *Journal of the American Chemical Society*, 2013, 135(4): 1349–1357.
[84] M. Vafaie, A. M. Najarian, J. Xu, L. J. Richter, R. Li, Y. Zhang, *et al*., "Molecular surface programming of rectifying junctions between InAs colloidal quantum dot solids," *Proceedings of the National Academy of Sciences*, 2023, 120(41): e2305327120.
[85] D. Shin, H. Jeong, J. Kim, E. Jang, Y. Park, and S. Jeong, "High performance infrared InAs colloidal quantum dot photodetector with 79% EQE enabled by an extended absorber layer," *Advanced Optical Materials*, 2025, 13(1): 2401931.
[86] J. H. Kim, B. K. Jung, S. K. Kim, K. R. Yun, J. Ahn, S. Oh, *et al*., "Ultrasensitive near-infrared InAs colloidal quantum dot-ZnON hybrid phototransistor based on a gradated band structure," *Advanced Science*, 2023, 10(18): 2207526.
[87] B. K. Jung, H. Yoo, B. Seo, H. J. Choi, Y. K. Choi, T. H. Kim, *et al*., "High-affinity ligand-enhanced passivation of group III-V colloidal quantum dots for sensitive near-infrared photodetection," *ACS Energy Letters*, 2024, 9(2), 504–512.
[88] T. Sheikh, W. J. Mir, A. Alofi, M. Skoroterski, R. Zhou, S. Nematulloev, *et al*., "Surface-reconstructed InAs colloidal nanorod quantum dots for efficient deep-shortwave infrared emission and photodetection," *Journal of the American Chemical Society*, 2024, 146(42): 29094–29103.
[89] M. J. Si, S. Jee, M. Yang, D. Kim, Y. Ahn, S. Lee, *et al*., "Colloidal InAs quantum dot-based infrared optoelectronics enabled by universal dual-ligand passivation," *Advanced Science*, 2024, 11(13): 2306798.
[90] H. J. Choi, B. K. Jung, Y. K. Choi, Y. K. Hong, Y. M. Lee, T. Park, *et al*., "Hydrogen chloride treated InAs quantum dot thin film phototransistor for ultrahigh responsivity," *Chemical Engineering Journal*, 2024, 499: 156191.
[91] H. W. Ban, M. Vafaie, L. Levina, P. Xia, M. Imran, Y. Liu, *et al*., "Resurfacing of InAs colloidal quantum dots equalizes photodetector performance across synthetic routes," *Journal of the American Chemical Society*, 2024, 146(36): 24935–24944.
[92] P. Xia, S. Wang, Y. Chen, A. Gulsaran, Y. Zhang, M. Vafaie, *et al*., "Improved facet and edge passivation in near-infrared III-V colloidal quantum dot photodetectors," *Advanced Materials*, 2025, 37(18), 2419020.
[93] J. Leemans, V. Pejović, E. Georgitzikis, M. Minjauw, A. B. Siddik, Y. H. Deng, *et al*., "Colloidal III-V quantum dot photodiodes for short-wave infrared photodetection," *Advanced Science*, 2022, 9(17): 2200844.
[94] H. Roshan, D. Zhu, D. Piccinotti, J. Dai, M. De Franco, M. Barelli, *et al*., "Near infrared light-emitting diodes based on colloidal InAs/ZnSe core/thick-shell quantum dots," *Advanced Science*, 2024, 11(23), 2400734.
[95] X. Zhao, L. J. Lim, S. S. Ang, and Z. K. Tan, "Efficient short-wave infrared light-emitting diodes based on heavy-metal-free quantum dots," *Advanced Materials*, 2022, 34(45): 2206409.
[96] B. Li, Y. Wang, J. Zhang, Y. Li, B. Li, Q. Lin, *et al*., "Efficient and stable near-infrared InAs quantum dot light-emitting diodes," *Nature Communications*, 2025, 16(1): 2450.
[97] D. Yuan, Z. Han, F. Cao, X. Liu, M. Liu, L. Zhang, *et al*., "Mixed halide passivation of $AgBiS_2$ quantum dots for high-performance photodetectors," *ACS Applied Electronic Materials*, 2024, 6(11):

8455–8462.

[98] X. Wang, Z. Song, H. Tang, Y. Li, H. Zhong, J. Wu, *et al*., "Synergic surface modifications of PbS quantum dots by sodium acetate in solid-state ligand exchange toward short-wave infrared photodetectors," *ACS Applied Materials & Interfaces*, 2024, 16(33): 44164–44173.

[99] P. Kumar, A. Salunke, S. Kumar, and S. Pradhan, "Ultralow dark current in lead sulfide colloidal quantum dots near-infrared photodetectors achieved through trap passivation with efficient surface ligands attachment," *ACS Applied Electronic Materials*, 2024, 6(12): 9113–9121.

[100] A. Sharma, H. Kim, G. Kim, J. Kang, C. B. Lee, S. Y. Bae, *et al*., "Dual facet passivation of silver halometallate for eco-friendly silver bismuth sulfide near IR photodetector," *Chemical Engineering Journal*, 2023, 473: 145246.

[101] A. B. Siddik, E. Georgitzikis, W. Song, A. Papadopoulou, A. U. Zaman, M. J. Lim, *et al*., "PbS and InAs quantum-dot thin films for short-wave infrared detectors," *ACS Applied Nano Materials*, 2024, 7(22): 25412–25422.

[102] H. Jo and M. S. Kang, "Ligand engineering for Indium-Based III-V semiconductor nanocrystals: a review on recent process," *Korean Journal of Chemical Engineering*, 2024, 41(13): 3431–3448.

[103] C. Maduwanthi, C. A. Jong, W. S. Mohammed, and S. H. Hsu, "Stability and photocurrent enhancement of photodetectors by using core/shell structured $CsPbBr_3/TiO_2$ quantum dots and 2D materials," *Nanoscale Advances*, 2024, 6(9): 2328–2336.

[104] Y. Liu, C. Zhao, J. Li, S. Zhao, X. Xu, H. Y. Fu, *et al*., "Highly sensitive $CuInS_2$/ZnS core-shell quantum dot photodetectors," *ACS Applied Electronic Materials*, 2021, 3(3): 1236–1243.

[105] M. C. Yen, Y. C. Yao, C. J. Lee, S. H. Huang, W. J. Hong, Y. Kajino, *et al*., "Color-filter-free image sensor using $CsPbBr_3$ quantum-dot-based Tamm plasmon photodetector for photonic synapse facial recognition," *Advanced Science*, 2025, 12(33): e03464.

[106] C. Kiguye, J. Jeong, and G. Kim, "Enhanced performance of polymer photodetectors using a metal-doped zinc oxide interfacial layer," *ACS Applied Materials & Interfaces*, 2025, 17(2): 4239–4246.

[107] S. Shim, S. Kim, D. Lee, H. Kim, M. J. Kwon, S. Cho, *et al*., "Infrared-triggered retinomorphic artificial synapse electronic device containing multi-dimensional van der Waals heterojunctions," *Small*, 2025, 21(24): 2410892.

[108] A. B. Siddik, W. Song, E. Georgitzikis, M. Vildanova, M. Jin, F. Berghmans, *et al*., "InAs colloidal quantum dot photodiode stack for CMOS-integrated infrared imaging," *ACS Nano*, 2025, 19(36): 32780–32787.

[109] J. Liu, Q. Liu, L. Huang, and M. Gong, "High energy eye-safe and mid-infrared optical parametric oscillator," *Laser Physics Letters*, 2010, 7(12): 853.

[110] Y. Wang, H. Wu, C. Rodà, L. Peng, N. Taghipour, M. Dosil, *et al*., "Shortwave infrared light detection and ranging using silver telluride quantum dots," *Advanced Materials*, 2025, 37(21): 2500977.

[111] L. Peng, Y. Wang, Y. Ren, Z. Wang, P. Cao, and G. Konstantatos, "InSb/InP core-shell colloidal quantum dots for sensitive and fast short-wave infrared photodetectors," *ACS Nano*, 2024, 18(6): 5113–5121.

[112] S. Chatterjee, K. Nemoto, H. T. Sun, and N. Shirahata, "Rational ligand design for enhanced carrier mobility in self-powered SWIR photodiodes based on colloidal InSb quantum dots," *Nanoscale Horizons*, 2024, 9(5): 817–827.

[113] S. Chatterjee, K. Nemoto, B. Ghosh, H. T. Sun, and N. Shirahata, "Solution-processed InSb quantum dot photodiodes for short-wave infrared sensing," *ACS Applied Nano Materials*, 2023, 6(17): 15540–15550